Energy flexibility curves to characterize the residential space cooling sector: The role of cooling technology and emission system

ENERGY FLEXIBILITY CURVES TO CHARACTERIZE THE RESIDENTIAL SPACE COOLING SECTOR: THE ROLE OF COOLING TECHNOLOGY AND EMISSION SYSTEM

Alice Mugnini[1*], Fabio Polonara[1,2], Alessia Arteconi[3,1]

[1]Dipartimento di Ingegneria Industriale e Scienze Matematiche, Università Politecnica delle Marche, Via Brecce Bianche 12, 60131, Ancona, Italy
[2]Istituto per le tecnologie della costruzione, Consiglio Nazionale delle Ricerche, Viale Lombardia 49, 20098, San Giuliano Milanese (MI), Italy
[3]Department of Mechanical Engineering, KU Leuven, B-3000, Leuven, Belgium

Email: *a.mugnini@univpm.it, f.polonara@univpm.it, a.arteconi@univpm.it

ABSTRACT

Space cooling of buildings shows an increasing trend in energy use worldwide. The exploitation of the energy flexibility reserve obtainable from buildings cooling-loads management can have an important role to improve the security and the reliability of the electricity power grid. Many studies in literature assess the energy flexibility potential of air conditioning systems; however, the role of the specific cooling technology is always scarcely explored. The objective of this work is to provide an evaluation of the operational energy flexibility that can be obtained involving the most common residential space cooling technologies, paying particular attention to the distribution system (e.g., all-air system, fan-coil units with and without the addition of a thermal energy storage and hydronic massive systems). The analysis is carried out with dynamic simulation models for the various cooling systems involved. Results show a great influence of the adopted distribution system in the implementation of a flexibility request. In particular, all-air systems (i.e. split systems) show the lower flexible behavior (they require up to 10 hours of precooling to be off during a peak hour). Whereas the adoption of fan coil units coupled with a thermal energy storage allows to implement different peak shaving strategies without compromising the indoor air temperature with low drawback effects in terms of anticipated electricity overconsumptions (no precooling of the air is required and a maximum of 23 % increase in electricity consumed in the time before the event occurs, with a reduction of 16 % in subsequent hours). In case of ceiling cooling systems, results highlight that as the thermal inertia of the system increases, the indoor conditions are less affected, but the anticipated overconsumption of the heat pump increases (for the same Demand Response event the electricity overconsumption goes from + 67 % to + 116 %, passing from ceiling panels to concrete ceiling). The results obtained from this analysis are then used to draw flexibility curves, which aim at providing a characterization of the flexibility of a cooling system. They can be used to predict, for typical installations, the system behavior in presence of a peak power reduction strategy in terms of pre-cooling duration, energy use variation and modification of the temperature comfort bandwidth. Such predictions are important because they can provide insights on the design and operation of space cooling systems in demand side management strategies.

Keywords: Energy Flexibility, Demand Response, Peak Shaving, Space Cooling, Thermal Distribution System

1. INTRODUCTION

Energy demand for space cooling (SC) has more than tripled worldwide since 1990, making it the fastest-growing end use in buildings [1]. In particular, the residential sector represents the 20 % of the final energy consumption [2]. To enable the use of a large share of renewable energy sources in the electricity generation mix, Demand Side Management (DSM) programs applied to buildings cooling loads can have a paramount role to improve the security of the power grid. DMS is defined as the set of actions aimed at planning, implementing and monitoring of utility activities designed to influence customers' use of electricity [3]. Between them, Demand Response (DR) strategies are considered one of the main solutions to alleviate the issues due to the unpredictability of generation, as they allow the exploitation of the latent flexibility of electrical demand [4]. In particular, a DR event represents a change in electric usage of the end-user from its normal consumption pattern in response to (i) changes in the price of electricity over time, or to (ii) incentive payments designed to induce lower electricity use at times of high wholesale market prices or when system reliability is jeopardized [5].

By virtue of the possible presence of different levels of thermal energy storage, buildings contain a relatively large share of demand that can be controlled, adapted and/or enhanced to produce energy flexibility services [6]. Focusing on cooling demand, there are several studies that investigate the potential load-shifting capability of the sector, demonstrating the relevance of this application. Many of them are mainly focused on the evaluation of the energy flexibility performance of the specific case studies analysed. For instance, Li et al. [7] investigated the couple effect of the thermal mass of a commercial building and its air-conditioning system for the realization of DR events. Modelling the dynamic of both the building and the air conditioning system with a white box approach, they obtained an electricity peak reduction of about 17 % with an on-off control and an additional reduction of about 2 % when also the chilled water temperature is controlled. Yan et al. [8] introduced a novel type of multi-timescale cold storage system to activate the energy flexibility of buildings cooling loads. The storage consists of a heat pipe-based natural ice storage subsystem and a dual-operation chiller. They applied the system to a building in Beijing (China) and evaluate an immediate power reduction by 41 % in response to the real-time DR during the peak cooling period on the design day. Arteconi et al. [9] evaluated the benefit of using a Thermal Energy Storage (TES) coupled with heat pumps for the realization of load shifting strategies in cooling season in an industrial building. They evaluated a charging time of 70 hours for the TES if the cold energy produced in the weekends and outside the working hours is used to cool it down. If fully charged, they calculated that the TES could satisfy the building cooling demand for more than one week. Tang et al. [10] demonstrated the capability of the air conditioning system of a commercial building to produce immediate power reductions. They implemented an optimized control logic that foresees the building cooling demand and determines the number and the regulation mode of operating chillers/pumps to be involved during the DR event. With their proposed strategy a 23 % reduction in power can be obtained, maintaining an acceptable zone temperature.

Other studies, instead, evaluate the potential load-shifting that can be obtained by the aggregated demand of the air conditioning sector. For example, Malik et. al [11] estimated possible peak load reductions of clusters of residential air-conditioning systems. Using monitored data of a large group of users (808 Australian household dwellings), they evaluated peak demand reductions from 4 to 9 % for the whole New South Wales State when different air-conditioner usage patterns are clustered. Qi et al. [12], introduced a three-stage load decomposition method based on clustering and correlation methodologies to disaggregate the whole-house energy consumption into Air Cooling (AC) loads and baseloads (loads not sensitive to temperature). They considered different usage patterns for the AC systems (a total of 19 patterns). Results suggested that the operational DR potential of the AC loads is more reliable and suitable to generate strategies for day ahead scheduling. Huang and Wu [13] presented an analytical method to build an aggregate flexibility model from residential AC systems for building-to-grid integration based on the virtual battery model. The simplified representation of building thermal dynamics in the analytical method is validated with highly reliable models developed in Modelica and Energy Plus. They estimated their analytical method valuable for power system operators to effectively coordinate a large number of flexible building assets with other resources.

As demonstrated by the papers cited above, the topic of the energy flexibility obtainable from the management of cooling loads in buildings has received considerable interest from the scientific community. However, the analysis is always focused on the description of a specific application or on the evaluation of the impact of the whole sector, without providing details about the single technologies composing the demand. The role of the particular space cooling technology in the realization of DR events is almost never highlighted. Instead, due to different intrinsic characteristics

that a cooling system can have (e.g., the thermal inertia of the distribution system, the rapidity in demand satisfaction or the accuracy in the comfort parameters control), it could have a great impact in the way the flexible event is carried out. Therefore, the objective of this paper is to provide an evaluation of the operative load-shifting capability of the most common residential space cooling technologies with a focus on the role of the indoor terminal units adopted.
Electric cooling systems are considered (e.g. on-off and variable capacity heat pumps) and three macro-categories of thermal distribution systems are modelled: all-air systems, fan-coil units and hydronic ceiling cooling systems. In particular five space cooling technologies are evaluated: split system with on-off regulation, fan coil units with and without the addition of a sensible TES, ceiling panels with an indoor air dehumidifier and a concrete ceiling cooling system coupled with an air dehumidifier.
The idea behind this study is to extend the design energy flexibility evaluation [14], already investigated by the authors in a previous work [15], to the operational scenario by analysing the working conditions of space cooling emission systems. In addition, flexibility curves for each emission system are proposed as an evaluation tool. These curves allow to characterize the behaviour of each system in terms of response to different events with an imposed load variation. They can be considered as an instrument to define guidelines for resources planning and Demand Side Management strategies. Furthermore, they can provide more technical insights on the specifications of such systems to support their design as energy flexibility enablers.

2. METHODOLOGY

With the aim of considering all the most widespread technologies at residential level, five different space cooling systems are modelled (Figure 1): an air to air heat pump with on-off regulation (split system, SS), an air to water heat pump with fan coil units (FCUs) as distribution system (this configuration is modelled both with and without the addition of a sensible thermal energy storage, TES) and an air to water heat pump coupled with two different hydronic ceiling distribution systems (ceiling panels, CP, and concrete ceiling cooling, CC). The latter two differ in their level of thermal inertia. The first one (CP, Figure 1(d)) is composed of pipes set on panels in the first internal layer of the roof (medium thermal inertia system) while the cooling concrete ceiling (CC, Figure 1(e)) has high storage capability, since its pipes are embedded in a high massive concrete layer.

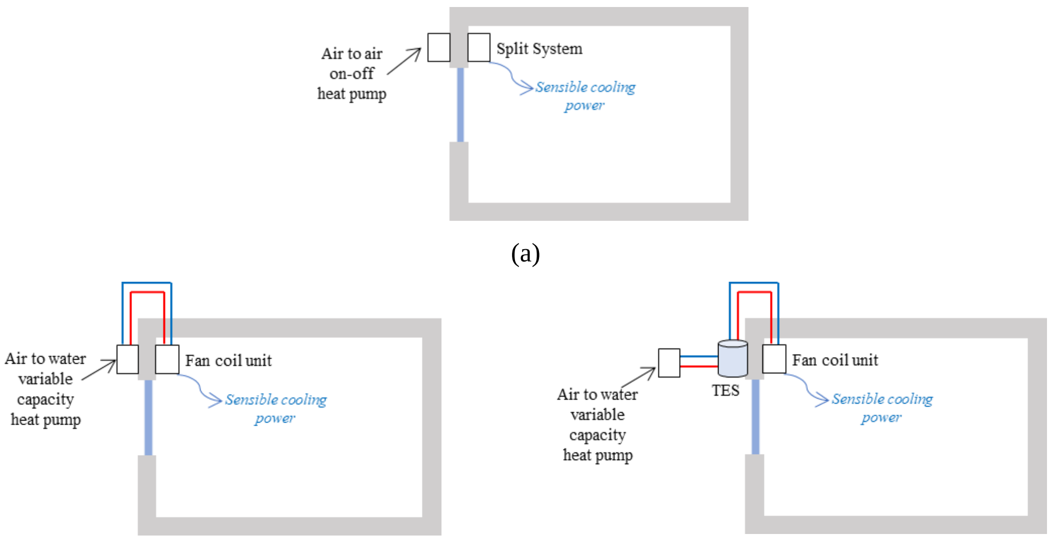

(a)

(b) (c)

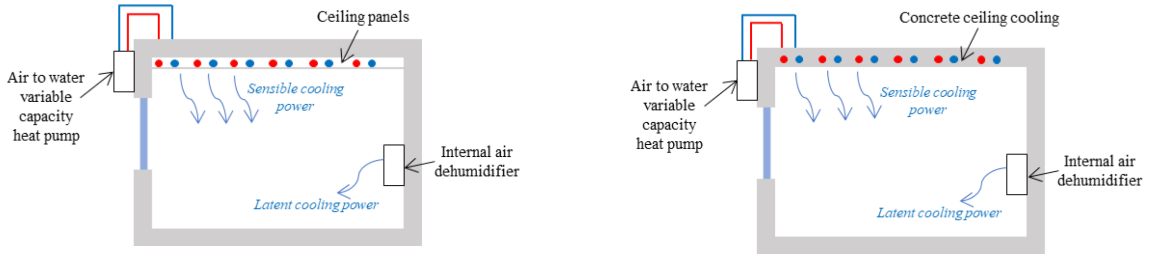

(d) (e)

Figure 1. Schematic of the modelled space cooling technologies: (a) split system; (b) variable capacity air to water heat pump with fan coil unit; (c) variable capacity air to water heat pump with fan coil unit equipped with TES; (d) variable capacity air to water heat pump with ceiling panels and dehumidifier and (e) variable capacity air to water heat pump with concrete ceiling cooling and dehumidifier.

When split systems and fan coil units are used, only the internal temperature can be directly controlled as comfort condition (with an indirect control over humidity through low supply temperature) while, in case of ceiling systems (CC and CP), a relative humidity punctual control must also be provided in order to guarantee a comfortable environment. Therefore, for these cases, the treatment of latent heat is entrusted to an internal air dehumidifier (DH). Table 1 reports the five considered cooling systems with a description of their main characteristics in terms of comfort parameters control, rapidity of satisfying the thermal demand and energy storage capacity.

Table 1. Space cooling technologies modelled and their main characteristics.

SC characteristics	SS	FCU	FCU with TES	CP	CC
Generation system	Air to air HP with on-off regulation	Air to water variable capacity HP	Air to water variable capacity HP	Air to water variable capacity HP and dehumidifier	Air to water variable capacity HP and dehumidifier
Distribution system	Internal unit of split system	Fan coil units (low supply temperature)	Fan coil units with TES (low supply temperature)	Ceiling panels (high supply temperature)	Concrete ceiling cooling (high supply temperature)
Comfort parameters controlled	Temperature	Temperature	Temperature	Temperature and humidity	Temperature and humidity
Rapidity of demand satisfaction	High	High	High	Medium	Low
Storage capability	Absent	Absent	From low to high in relation to the TES size	Medium-low	High

The description of the modeling approach adopted to obtain the dynamic behavior of each cooling system is reported in Section 2.1, where details about the building model are included. A building with the same thermal and geometrical properties is considered for all the space cooling systems, thus alleviating the influence of the building characteristics on the comparison analysis. Then, in Section 2.2, the Demand Response events are described and details about their formulation and implementation are provided. Finally, in Section 2.3, some parameters to evaluate the operational flexibility are introduced: they are adopted to build the flexibility curves in order to provide an instrument to easily compare the performance of the different cooling systems under different points of views.

2.1 Thermal model of the space cooling systems

In order to model the building thermal dynamics, a detailed (10 thermal resistances and 7 thermal capacitances) lumped-parameter model based on the thermal-electricity analogy is used [16]. A common structure is used for all the space cooling technologies (Figure 2). The parameters of the network of thermal resistances and capacitances (RC-network) are identified with a white box approach according to the thermal and geometrical characteristics of a reference building. In Figure 2 is represented the thermal conductance (K), defined as the reciprocal of thermal resistance.

To represent the short-term dynamic of a building with good performance accuracy and low computational cost, each opaque surface of the building envelope is modelled with two capacitances (thermal nodes) and three thermal resistances according with the model architecture proposed by Boodi et al. [17]. In particular, the two thermal capacities represent all the layers of the surface in the positions preceding and following the thermal insulation. Consequently, the two temperatures are the surface temperatures of the insulation layer. The numerical values of thermal resistances (R) and capacitances (C) are calculated taking inspiration from the approach proposed in EN ISO 13790 standard [18] (developed for a simple 5R1C building model). The numerical values of the parameters are reported in Section 3 where the case study is described.

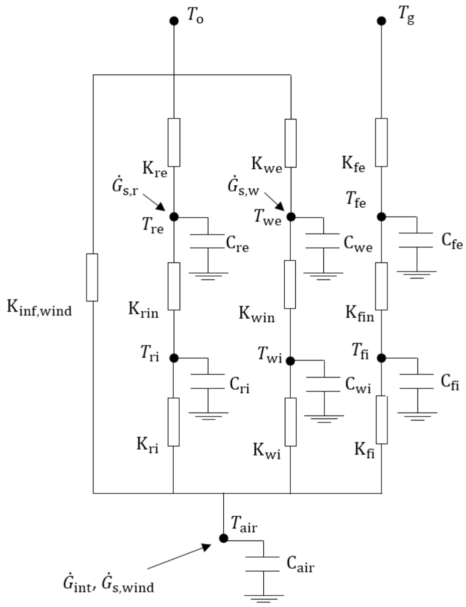

Figure 2. 10R7C network building model.

Assuming one-dimensional heat transfer, the system dynamics can be described as a classic linear state-space model:

$$\mathrm{d}\boldsymbol{X}(\mathrm{t}) = \mathbf{A} \cdot \boldsymbol{X}(\mathrm{t})\mathrm{dt} + \mathbf{B} \cdot \boldsymbol{U}(\mathrm{t})\mathrm{dt} \quad \text{Eq. 1}$$

$$\boldsymbol{Y}(\mathrm{t}) = \mathbf{C} \cdot \boldsymbol{X}(\mathrm{t})\mathrm{dt} + \mathbf{D} \cdot \boldsymbol{U}(\mathrm{t})\mathrm{dt} \quad \text{Eq. 2}$$

where $\boldsymbol{X}(t)$ is the state-space vector, $\boldsymbol{U}(t)$ is the input vector and $\boldsymbol{Y}(t)$ represents the output vector. **A**, **B**, **C** and **D** are time-invariant real matrices depending on the parameters of the network.

As can be noted in Figure 2, the contribution of the cooling system ($\dot{Q}_{\mathrm{SC}}$) is not shown, since the way it is supplied depends on the specific space cooling technology. Indeed, when the cooling system is composed of an air distribution system (e.g. split systems and fan coil units), $\dot{Q}_{\mathrm{SC}}$ is directly removed from the internal air node temperature (T_{air}). Instead, in case of addition of a thermal energy storage to the fan coil water circuit, the thermal power that is supplied to the internal air thermal node ($\dot{Q}_{\mathrm{building}}$) is decoupled from that produced by the cooling system ($\dot{Q}_{\mathrm{SC}}$). Their link is formalized in the thermal energy storage (TES) model (Equation 3) [19]:

$$\mathrm{C}_{\mathrm{TES}} \cdot \frac{\mathrm{d}T_{\mathrm{TES}}}{\mathrm{dt}} = \dot{Q}_{\mathrm{SC}} + \dot{Q}_{\mathrm{building}} + \mathrm{L}_{\mathrm{TES}}(T_{\mathrm{env}} - T_{\mathrm{TES}}) \quad \text{Eq. 3}$$

The TES is assumed to be a perfectly mixed water tank. Its storage capability is modelled with a thermal capacitance ($\mathrm{C}_{\mathrm{TES}}$) and with a temperature node (T_{TES}). The thermal losses with the environment temperature (T_{env}) are modelled with a loss coefficient factor (L_{TES}). Although Equation 3 introduces an approximation in the modeling of the tank (i.e. the stratification is neglected) this is considered acceptable for the purposes of the analysis proposed in this work since, dealing with the summer case, the temperature difference granted to the tank is quite small (5 ° C as will be seen in Section 3).

In case of ceiling cooling systems (ceiling panels, CP, and concrete ceiling cooling, CC), $\dot{Q}_{SC}$ is removed from the inner roof thermal node. In case of high massive system (CC) this node coincides with the node T_{ri} in Figure 2, while for the ceiling panels (CP) a further thermal node for the ceiling is distinguished ($T_{ri,cp}$, which stands for the position immediately after the internal plaster, in Figure 3).

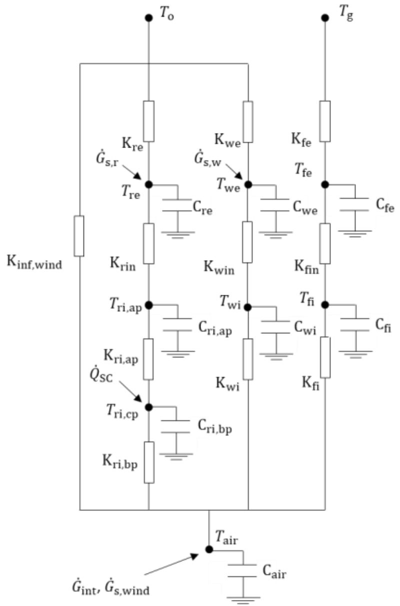

Figure 3. 11R8C network for CP system sensible model.

In these last two space cooling systems (CC and CP), also the humidity control is enabled. With reference to the effective capacitance humidity model [20], the moisture balance is carried out in parallel with the sensible energy balance calculation. For the air node it is expressed as:

$$M_{air} \frac{dx_{air}}{dt} = \dot{m}_{vent}(x_o - x_{air}) + \frac{\dot{Q}_{DH}}{h_v} \qquad \text{Eq. 4}$$

Where M_{air} and x_{air} are the mass and the absolute humidity of the internal air, $\dot{m}_{vent}$ and x_o are the natural ventilation flowrates and its absolute humidity, $\dot{Q}_{DH}$ is the latent contribution of the dehumidifier systems and h_v is the heat of evaporation of water (approximately assumed constant in the balance).

2.2 Demand Response event

The capability of a space cooling system to respond to a programmed load variation is evaluated by simulating different Demand Response events and comparing them with a reference case (Baseline). The Baseline (BL) is represented by the demand curve of each cooling system able to maintain the comfort conditions. It is computed as the solution of a linear optimization problem that has the objective of minimizing the thermal requirement of the building:

$$\text{minimize}\left(\sum_{k_{start}}^{k_{end}} \dot{Q}_{SC}(k) \cdot \Delta k\right) \qquad \text{Eq. 5}$$

where k is the discrete time and Δk the simulation timestep, which has been set equal to 0.1 hours (6 minutes). Here, the thermal power of the cooling system ($\dot{Q}_{\mathrm{SC}}$) is the decision variable of the optimization problem and it is limited at each timestep (Δk) by the maximum power of the generating system. A distinction has to be made between the optimization problem solved for the split system (i.e., on/off regulation) and the other cooling systems (i.e., FCU, CP and CC). Actually, if for the FCU, CP and CC systems a typical linear programming optimization problem is written (Equation 5), for the split a MILP (mixed-integer linear programming) is introduced to reproduce the on-off regulation. In this case, the optimization problem is represented in Equation 5 as:

$$\text{minimize}\left(\sum_{\mathrm{k_{start}}}^{\mathrm{k_{end}}} \dot{\mathrm{Q}}_{\text{full-load}}(k)\cdot CTRL_{\mathrm{SS}}(k)\cdot\Delta\mathrm{k}\right) \qquad \text{Eq. 6}$$

where $CTRL_{\mathrm{SS}}$ is the Boolean decision variable for the split system and it is limited at each timestep by the maximum power of the generating system ($\dot{\mathrm{Q}}_{\text{full-load}}$).

The comfort constraints on the air temperature node must be satisfied. They are modelled with a setpoint temperature ($\mathrm{T_{sp}}$) and an allowed comfort band defined with a $\Delta T_{\mathrm{sp,max}}$ (upper comfort band) and a $\Delta T_{\mathrm{sp,min}}$ (lower comfort band):

$$\forall\, k \quad \left(\mathrm{T_{sp}}-\Delta T_{\mathrm{sp,min}}(k)\right)\leq T_{\mathrm{air}}(k)\leq\left(\mathrm{T_{sp}}+\Delta T_{\mathrm{sp,max}}(k)\right) \qquad \text{Eq. 7}$$

Moreover, if the cooling system is able to control also the internal humidity, the same condition expressed in Equation 7, can be written for the relative humidity (RH):

$$\forall\, k \quad (\mathrm{RH_{sp}}-\Delta RH_{\mathrm{sp,min}}(k))\leq RH(k)\leq(\mathrm{RH_{sp}}+\Delta RH_{\mathrm{sp,max}}(k)) \qquad \text{Eq. 8}$$

The constraint formulated in Equation 8, is actually mathematically expressed in terms of absolute humidity (x). Therefore, the effective constraint is:

$$\forall\, k \quad x_{\mathrm{min}}(k)\leq x_{\mathrm{air}}(k)\leq x_{\mathrm{max}}(k) \qquad \text{Eq. 9}$$

With x_{min} and x_{max} calculated as the absolute humidity at the allowed upper comfort limit for the temperature ($\mathrm{T_{sp}}+\Delta T_{\mathrm{sp,max}}$) and respectively the lower ($\mathrm{RH_{sp}}-\Delta RH_{\mathrm{sp,min}}$) and the upper ($\mathrm{RH_{sp}}+\Delta RH_{\mathrm{sp,max}}$) comfort limit for the relative humidity.

When the cooling power is not directly provided to the internal air node (T_{air}) (e.g., for fan coil units coupled with TES, ceiling panels or cooling concrete ceiling systems), a constraint on the temperature of the thermal mass (TMD) of the distribution system node is required:

$$\forall\, k \quad \mathrm{T_{TMD,min}}\leq T_{\mathrm{TMD}}(k)\leq\mathrm{T_{TMD,max}} \qquad \text{Eq. 10}$$

In particular, T_{TMD} coincides with T_{TES} for the cooling system composed of fan coil units and TES, $T_{\mathrm{ri,cp}}$ for ceiling panels and T_{ri} for concrete ceiling cooling system.

The Demand Response event is a peak shaving strategy (PSS). It is modeled by imposing at a certain time $\mathrm{k_{start,DR}}$ and for a period $\Delta\mathrm{k_{DR}}$ a variation of the electrical power peak of the Baseline, according to a reduction factor ($\mathrm{f_{PSS}}$).

$$\text{For } \mathrm{k_{start,DR}}\leq k\leq\mathrm{k_{end,DR}} \quad \dot{P}_{\mathrm{DR}}=\mathrm{f_{PSS}}\cdot\dot{P}_{\mathrm{max,BL}} \qquad \text{Eq. 11}$$

With: $\mathrm{k_{end,DR}}=\mathrm{k_{start,DR}}+\Delta\mathrm{k_{DR}}$

This condition is modelled as an additional constraint for the optimization problem:

$$\forall\, k \quad \dot{P}_{\mathrm{SC}}(k)\leq\dot{P}_{\mathrm{DR}}(k) \qquad \text{Eq. 12}$$

where $\dot{P}_{\mathrm{SC}}$ is the electrical absorption of the individual cooling systems. The condition imposed by Equation 12 is converted in terms of a constraint on the thermal power, by means of the knowledge of the heat pump performance function (*EER*), which depends on the external temperature, supply temperature and capacity ratio and that is known at the time of the DR event.

To ensure a certain level of flexibility to all the space cooling technologies, the exploitation of the energy flexibility provided by thermostatic controlled loads (TCLs) is used in case of Demand Response event. Let be $\Delta T_{\mathrm{sp,max,BL}}$ and $\Delta T_{\mathrm{sp,min,BL}}$ the upper and the lower tolerance bands for setpoint in BL, the flexibility from TCLs is activated in case of DR by allowing the air node temperature (T_{air}) to drop down to a lower value (low comfort band, $\Delta T_{\mathrm{sp,min,DR}}$) or to rise to a higher value (high comfort bandwidth,$\Delta T_{\mathrm{sp,max,DR}}$) than those fixed in the Baseline. The exploitation of the temperature range $[\mathrm{T_{sp}} - \Delta T_{\mathrm{sp,min,DR}}; \mathrm{T_{sp}}]$ is always granted, while the upper interval $(\mathrm{T_{sp}}; [\mathrm{T_{sp}} + \Delta T_{\mathrm{sp,max,DR}}])$ is allowed only during the event ($\Delta \mathrm{k_{DR}}$). If also the humidity can be controlled by the cooling system, a $\Delta RH_{\mathrm{sp,max,DR}}$ and a $\Delta RH_{\mathrm{sp,min,DR}}$ are introduced with the same logic. Figure 4 reports a representation of the DR event in comparison with the relative Baseline. As it can be noted, since the aim is to assess the thermal demand needed to ensure the setpoint, in BL the value of $\Delta T_{\mathrm{sp,max,BL}}$ is always equal to 0 °C.

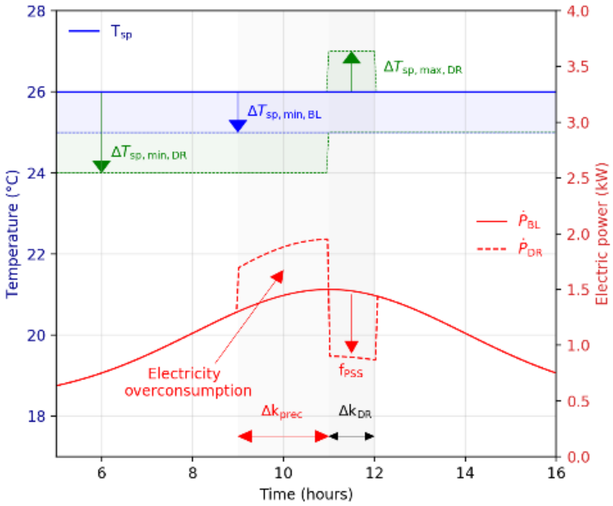

Figure 4. Representation of the generic Demand Response event modelled in comparison with the Baseline.

It is important to notice that although the modeling of the Demand Response event foresees a constraint on the electrical power of the system (Equation 12), the optimization problem is formulated in terms of minimization of the thermal requirement (Equation 5). This choice allows to take into consideration the variability of the *EER* in presence of a variable capacity heat pump and it allows to maintain the problem linear, without introducing any approximation which neglects the *EER* dependence on the boundary conditions and on the load, as normally done in literature.

2.3 Flexibility evaluation method

Since both the Baseline and the Demand Response operation are calculated through the resolution of an optimization problem, whether and how a space cooling technology carries out the event depends on the characteristics of its distribution system (Table 1). Therefore, to produce the same DR event, different sources of flexibility can be exploited by each cooling systems in different ways and with different results in terms of user involvement and variations in electricity demand. In particular, to quantify the ability of each system to be energy flexible, the following logic is pursued: a system is the more flexible the more it manages to carry out the Demand Response event with the least possible side effects in terms of comfort degradation and payback load [21] before and after the event. In order to propose a general methodology that allow to highlight the contribution of each physical variable involved in the event, different quantities are introduced to characterize the building response to the event:

(i) The use of the energy flexibility of the thermal mass of the distribution system (TMD). This quantity can be calculated only in cases in where the cooling power produced by the generation system is removed to a thermal node (T_{TMD}) different from the internal air node (T_{air}): therefore in case of FCU with the addition of the TES (T_{TMD} coincides with T_{TES}), CC (T_{TMD} coincides with T_{ri}) and CP (T_{TMD} coincides with $T_{\mathrm{ri,cp}}$). The strategy that can be implemented is the pre-cooling of this thermal mass in the hours preceding the event. To estimate this exploitation, the quantity $Flex_{\mathrm{TMD}}$ (in percentage) is calculated. It represents the variation between the Demand Response and the Baseline scenario of the temperature of the distribution system thermal mass (T_{TMD}), referred to the Baseline:

$$Flex_{\mathrm{TMD}} = \frac{T_{\mathrm{TMD,DR}} - T_{\mathrm{TMD,BL}}}{T_{\mathrm{TMD,BL}}} \qquad \text{Eq. 13}$$

(ii) The use of the energy flexibility of thermostatically controlled loads (TCLs). Again, the strategies that can be implemented are the pre-cooling of the internal air in the hours preceding the event and the raising of the temperature during the event ($\Delta \mathrm{k}_{\mathrm{DR}}$). To estimate this exploitation, the quantity $Flex_{\mathrm{TCL}}$ (in percentage) is calculated. It represents the variation between the Demand Response and the Baseline scenario of the temperature of the internal air thermal node (T_{air}), referred to the air temperature of the Baseline:

$$Flex_{\mathrm{TCL}} = \frac{T_{\mathrm{air,DR}} - T_{\mathrm{air,BL}}}{T_{\mathrm{air,BL}}} \qquad \text{Eq. 14}$$

If a humidity control is possible for the cooling system, the same quantity can be calculated for the relative humidity (*RH*):

$$Flex_{\mathrm{RH}} = \frac{RH_{\mathrm{DR}} - RH_{\mathrm{BL}}}{RH_{\mathrm{BL}}} \qquad \text{Eq. 15}$$

Furthermore, the pre-cooling time interval ($\Delta \mathrm{k}_{\mathrm{prec}}$) is calculated as the time period (before the DR event) in which the air temperature in Demand Response scenario is lower than in the Baseline.

(iii) The payback load in the electricity power curve. This effect can derive both from the use of the flexibility from thermostatically controlled loads and from the exploitation of the thermal inertia of the system. It is represented both by the electric power variation $\dot{P}^{*}_{\mathrm{shift}}$ ($\dot{P}_{\mathrm{rated}}$ represents the rated electricity power of the specific space cooling technology):

$$\dot{P}^{*}_{\mathrm{shift}} = \frac{\dot{P}_{\mathrm{DR}} - \dot{P}_{\mathrm{BL}}}{\dot{P}_{\mathrm{rated}}} \qquad \text{Eq. 16}$$

and also by the energy consumption variation (in percentage terms) in the time before and after the Demand Response event:

$$\mathrm{E}_{\mathrm{shift,bDR}} = \frac{\sum_{k=\mathrm{k_{strat}}}^{\mathrm{k_{strat,DR}}} \left(\dot{P}_{\mathrm{DR}}(k) - \dot{P}_{\mathrm{BL}}(k)\right) \Delta \mathrm{k}}{\sum_{k=\mathrm{k_{strat}}}^{\mathrm{k_{strat,DR}}} \dot{P}_{\mathrm{BL}}(k)\, \Delta \mathrm{k}} \qquad \text{Eq. 17}$$

$$\mathrm{E}_{\mathrm{shift,aDR}} = \frac{\sum_{k=\mathrm{k_{end,DR}}}^{\mathrm{k_{end}}} \left(\dot{P}_{\mathrm{DR}}(k) - \dot{P}_{\mathrm{BL}}(k)\right) \Delta \mathrm{k}}{\sum_{k=\mathrm{k_{end,DR}}}^{\mathrm{k_{end}}} \dot{P}_{\mathrm{BL}}(k)\, \Delta \mathrm{k}} \qquad \text{Eq. 18}$$

As it can be noted, the quantities introduced make it possible to evaluate which source of flexibility is exploited by the plant (i.e. TMD or TCLs) and to what extent this occurs. Thanks to the quantities presented, two levels of analysis are possible.

- The first allows to timely and punctually evaluate the behavior of the plant during the Demand Response event with reference to the baseline. Indeed, with $Flex_{\mathrm{TMD}}$, $Flex_{\mathrm{TCL}}$, $Flex_{\mathrm{RH}}$ it is possible to appreciate the extent of activation of the various sources of flexibility and thanks to $\dot{P}^{*}_{\text{shift}}$ their feedback on the temporal variation of the electric power can be assessed.

- On the other side, with the calculation of the parameters: $\Delta \mathrm{k}_{\text{prec}}$ (duration of the pre-cooling of the internal air), $\mathrm{E}_{\text{shift,bDR}}$ and $\mathrm{E}_{\text{shift,aDR}}$ (i.e. energy consumption variation in the time before and after the event), it is possible to summarize the impact on the user setpoint and on electricity demand.

It is precisely from the calculation of these two parameters under different Demand Response events (i.e. peak reduction amount) that the flexibility curves can be obtained. Therefore, the flexibility curves have the objective of characterizing the behavior of an emission system and they represent an instrument to quickly predict the response of the system.

3. DYNAMIC MODEL

A dynamic model to analyze the behavior of the different cooling systems has been developed. The latter are supposed installed in a typical Italian building, representative of the building stock. This choice helps to obtain results that can be easily generalized. The thermal characteristics of the building are extrapolated by Tabula Project [22]. In particular, a single-family house is selected with construction period after 2006. The value of the thermal transmittances of the single opaque and transparent surfaces are reported in Table 2. The stratigraphy and the materials composing the individual parts of the building envelope are chosen with reference to [23]. Hourly air changes of 0.2 h^{-1} are used and the internal gains (due to occupation and equipment) are evaluated with [18]. To obtain the environmental conditions (outdoor temperature and solar radiation), a climate file is adopted (Rome 41°53' N 12°28' E) [24].

Table 2. Thermal transmittances (U-value) for the single opaque and transparent surfaces of the building.

External walls ($W\ m^{-2}K^{-1}$)	**Roof ($W\ m^{-2}K^{-1}$)**	**Floor ($W\ m^{-2}K^{-1}$)**	**Windows ($W\ m^{-2}K^{-1}$)**
0.34	0.28	0.33	2.20

In case of presence of a thermal energy storage in the fan coil water circuit, a typical storage system suitable for heat pumps [25] of 750 liters (0.75 m^3) is introduced. Considering the Vitocell 100-E series (type SVP/SVPA), the catalog reports an internal diameter (without insulation) of 0.79 m and a thermal coefficient loss per area of 0.68 $W\ m^{-2}\ K^{-1}$. Since it is used for cooling its internal temperature (T_{TES}) will be in the range 7-12 °C (Equation 10). According to the same logic, also the temperature of the nodes from which heat is removed in the ceiling panels and in the cooling concrete ceiling systems ($T_{\text{ri,cp}}$ and T_{ri}) are limited in the interval 18-26 °C to avoid thermal discomfort.

Table 3 shows all the RC-network parameters values obtained for the case study.

Table 3. Numerical value of parameters.

Thermal conductance	**($W\ K^{-1}$)**	**Thermal capacity**	**($kWh\ K^{-1}$)**
$\mathrm{K}_{\text{inf,wind}}$	73.1	C_{we}	6.4
K_{we}	139.7	C_{wi}	2.5
K_{win}	51.2	C_{re}	4.7
K_{wi}	267.8	C_{ri}	7.4
K_{re}	1019.5	$\mathrm{C}_{\text{ri,ap}}$	6.7
K_{rin}	30.8	$\mathrm{C}_{\text{ri,bp}}$	0.8
K_{ri}	399.3	C_{fe}	21.1
$\mathrm{K}_{\text{ri,ap}}$	1909	C_{fi}	9.6
$\mathrm{K}_{\text{ri,bp}}$	504.9	C_{air}	0.1
K_{fe}	557.6	C_{TES}	0.9
K_{fin}	40.0		
K_{fin}	396.9		
K_{l}	3.2		

To model the cooling generation systems, a commercial variable capacity heat pump (HP) is selected (Vitocal B04/A04) [26]. It is an air to water heat pump of 3.8 kW_{th} and *EER* of 2.16 with a water supply temperature of 7 °C and an outdoor temperature of 35 °C (performances become 4.7 kW_{th} and *EER* of 2.71 with a water supply temperature of 18 °C and an outdoor temperature of 35 °C). For the on-off air-to-air heat pump, the full load performances of [26] with a flow temperature of 7 °C. For the fan coil model, the performances are evaluated with a supply temperature of 7 °C while for the ceiling distribution systems (CC and CP) it is fixed to 18 °C. Figure 5 shows the COP trend of the modelled heat pumps by varying the ambient temperature and the thermal capacity.

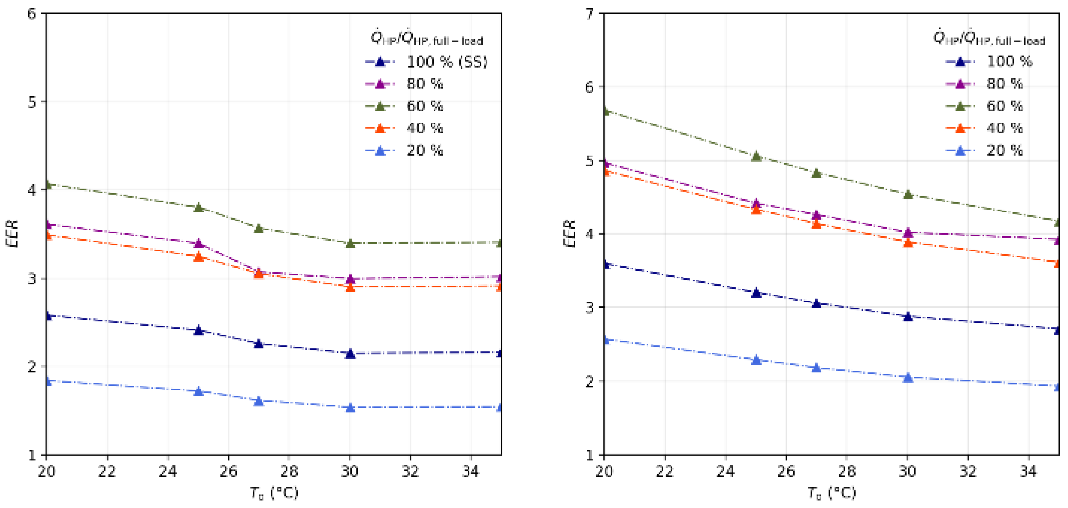

(a) (b)

Figure 5. Performance (*EER*) of the heat pumps by varying the outside temperature (T_o): (a) variable capacity heat pump for a fixed water supply temperature of 7 °C and (b) variable capacity heat pump for a fixed water supply temperature of 18 °C.

As mentioned, for the hydronic radiant cooling systems (CC and CP), it is possible to control also the humidity, by using an air dehumidifier (DH). Its characteristics are selected with references to commercial DH to be combined with ceiling systems [27]. In particular, the IN+ 300 model is chosen. It has a dehumidification capacity of 20.8 l day^{-1} with an electricity absorption of 320 W_e.

In Table 4 are summarized all the parameters used to simulate the space cooling technologies.

Table 4. Parameters used to simulate the cooling systems.

SS		**FCU**		**CP and CC**	
Heat pump		**Heat pump**		**Heat pump**	
Design supply temperature	7 °C	Design supply temperature	7 °C	Design supply temperature	18 °C
Thermal power (W7A35)	3.8 kW_{th}	Thermal power (W7A35)	3.8 kW_{th}	Thermal power (W18A35)	4.7 kW_{th}
COP (W7A35)	2.16	COP (W7A35)	2.16	COP (W18A35)	2.71
Regulation	On-off	Regulation	Power regulation from 30 % of maximum load	Regulation	Power regulation from 30 % of maximum load
TMD		**TMD**		**TMD**	
Location	Absent	Location	Available in case of TES addition	Location	Roof layer
		Constraints	7-12 °C	Constraints	18-26 °C
		Volume	75 liters		
DH		**DH**		**DH**	
Absent		Absent		Capacity	20.8 liters day^{-1}
				Electricity absorption	320 W_e

4. RESULTS

A summer representative day is selected to analyze the systems operation. It is selected as the day in which the average daily outdoor air temperature is closer to the daily monthly average outdoor air temperature of the wheatear data (5 July). By varying the day on which the event occurs, slightly different values are obtained, without affecting the overall conclusions. Thus the general considerations on the flexibility curves for the different emission systems remain valid regardless of the chosen day.

In the next paragraph (Section 4.1), the characteristics of the individual Space Cooling technologies in Demand Response scenarios will be described in relation to the relative Baseline; both the dynamic behavior and the flexibility curves are discussed. Then, in Section 4.2, a comparison between the various systems is provided.

4.1 Assessment of operational flexibility for the single Space Cooling technologies

In order to assess the punctual behavior of the single technology in a load-shifting scenario, the dynamic behavior of each cooling system is described firstly with reference to the same peak shaving event, and then under different conditions. In order to obtain a characterization as complete as possible of the load-shifting capability of the systems, the parameters that characterize the DR event (f_{PSS}, $\Delta T_{sp,max,DR}$, $\Delta T_{sp,min,DR}$, $\Delta RH_{sp,max,DR}$ and $\Delta RH_{sp,min,DR}$) are varied in the analysis. For simplicity, only Demand Response events that start at the peak time are considered ($k_{start,DR}$ equal to $k_{peak,BL}$). Moreover, although not very applicable in practice, except for more modern thermostats, variations in very narrow boundary conditions (i.e., 0.1 °C) for the setpoints ($\Delta T_{sp,max,DR}$ and $\Delta T_{sp,min,DR}$) are also tested in order to map the behavior of the individual systems.

4.1.1 Split System (SS) with on-off operation

When the cooling demand of the building is satisfied with an on-off split system (SS), the temperature of the air node (T_{air}) cannot be maintained at the constant value of the setpoint (T_{sp} of 26 °C) but it oscillates within the band allowed by the thermostat (Figure 6(a)). As can be seen from Figure 6(a), due to the intermittent operation of the heat pump it was necessary to set a rather high low tolerance to the setpoint ($\Delta T_{sp,min,BL}$ of 2 °C) throughout the day also in case of BL. In Figure 6(b) the thermal and electric power consumption of the heat pump in case of Baseline operation is shown. In particular, the daily cooling energy demand is 21.8 kWh_{th}, while the electricity consumption is 9.2 kWh_e. The electricity peak power is 0.84 kW_e and occurs at 2.00 pm.

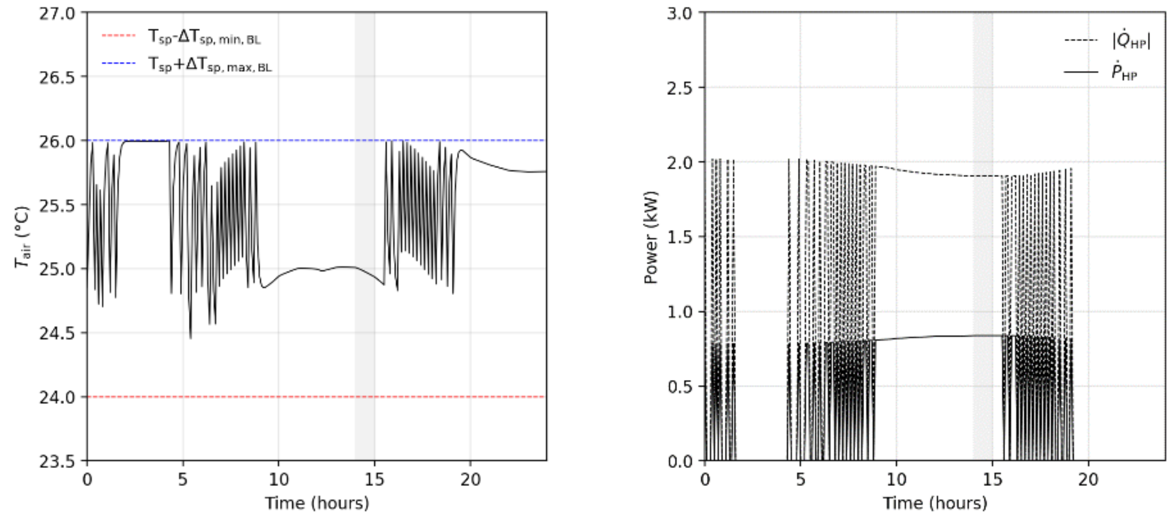

(a) (b)

Figure 6. Daily Baseline operation for SS with on-off regulation: (a) internal air node temperature and (b) thermal and electrical HP power.

Since no modulation of the heat pump can be exploited, only a Demand Response event with a reduction factor (f_{PSS}) equal to zero can be tested. It is not possible the realization of Demand Response events located at the peak ($k_{start,DR}$ equal to $k_{peak,BL}$) and lasting longer than a timestep (6 minutes) with $\Delta T_{sp,max,DR}$ equal to 0 °C. Accordingly, a certain upper comfort limit must be guaranteed during the event (i.e. $\Delta T_{sp,max,DR}$ different from 0 °C). In Figure 7 the behavior of the split system in term of the use of the energy flexibility of thermostatically controlled loads (Figure 7(a)) is represented, and the presence of payback loads in the electricity power curve (Figure 7(b)) when an event of 1 hour is tested with an upper comfort band ($\Delta T_{sp,max,DR}$) of 0.5 °C as well. As can be seen, the implementation of the event requires a large activation of the energy flexibility from TCLs. Indeed, the calculated pre-cooling time interval (Δk_{prec}) is about 10.2 hours and for all the duration of the event (area highlighted in gray in Figure 7(a)) all the upper comfort band ($\Delta T_{sp,max,DR}$) is exploited. Given the cycling of the system, it is difficult to compare the power trend in the Baseline and in the Demand Response scenario, therefore it is not possible to distinguish graphically the exact occurrence of payback loads (Figure 7(b)). Therefore, the planning of a strategy by a potential supervisor (aggregator) would appear rather complicated given the difficulty in predicting rapid sequences of on and off cycles in the period preceding the event. However, in the case showed in Figure 7, a + 28.7 % of $E_{shift,bDR}$ is calculated considering the time before the event, while a $E_{shift,aDR}$ of - 7.8 % is obtained considering the electricity variation after the DR event.

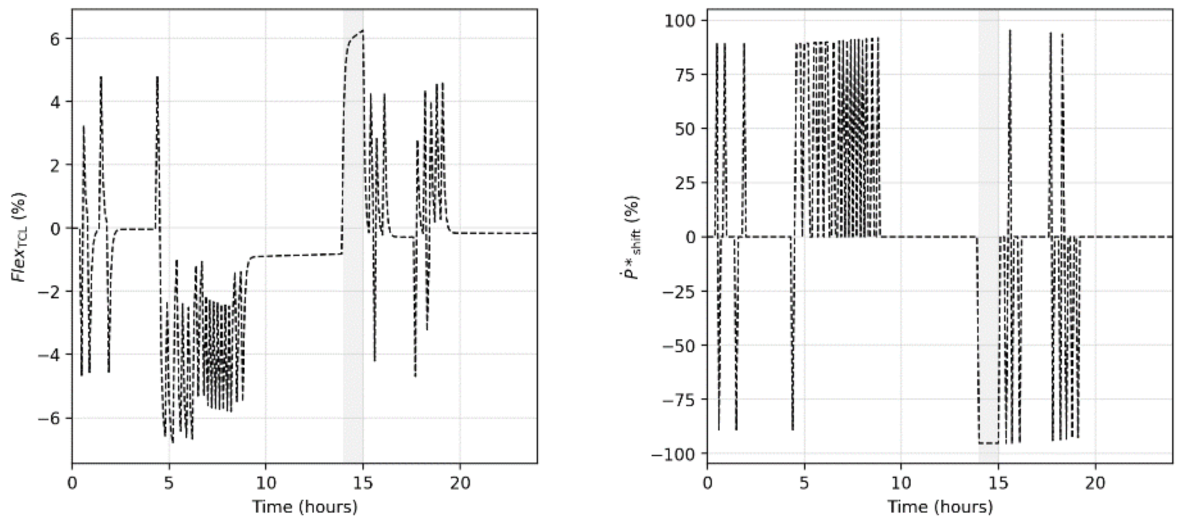

(a) (b)

Figure 7. Daily Demand Response operation (f_{PSS} equal to 0, Δk_{DR} of 1 hour, $\Delta T_{sp,min,DR}$ of 2 °C, $\Delta T_{sp,max,DR}$ of 0.5 °C and $k_{start,DR}$ coinciding with $k_{peak,BL}$) for SS with on-off regulation: (a) $Flex_{TCL}$ and (b) $\dot{P}^*_{shift}$.

Since, as mentioned, only Demand Response events with reduction factor (f_{PSS}) equal to 0 can be realized, the parameters that can be varied are the lower and the upper comfort bands (i.e. $\Delta T_{sp,min,DR}$ and $\Delta T_{sp,max,DR}$). Moreover, not all the thermostat variations allow to find a feasible solution for the optimization problem and therefore to realize the peak shaving event. Figure 8 reports the flexibility curves obtained for the split system. As can be noted, they are referred to a fixed value of lower comfort band ($\Delta T_{sp,min,DR}$ equal to 2 °C) as lower values are not feasible in the optimization problem (the split system appears rather inflexible in producing load variations).

By activating the energy flexibility from TCLs, the peak cannot be zero with an upper comfort band ($\Delta T_{sp,max,DR}$) lower than 0.3 °C. On the contrary, allowing higher upper comfort bands, the event can be realized with rather short times of pre-cooling of the air temperature (up to 0.6 °C for the $\Delta T_{sp,max,DR}$ the precooling is higher than 8.7 hours, while for higher values of $\Delta T_{sp,max,DR}$ the pre-cooling is always lower than 2.25 hours). Anyhow, given the limited number of possible cases for this type of cooling system, flexibility curves represent only the behavior in a few points (Figure 8).

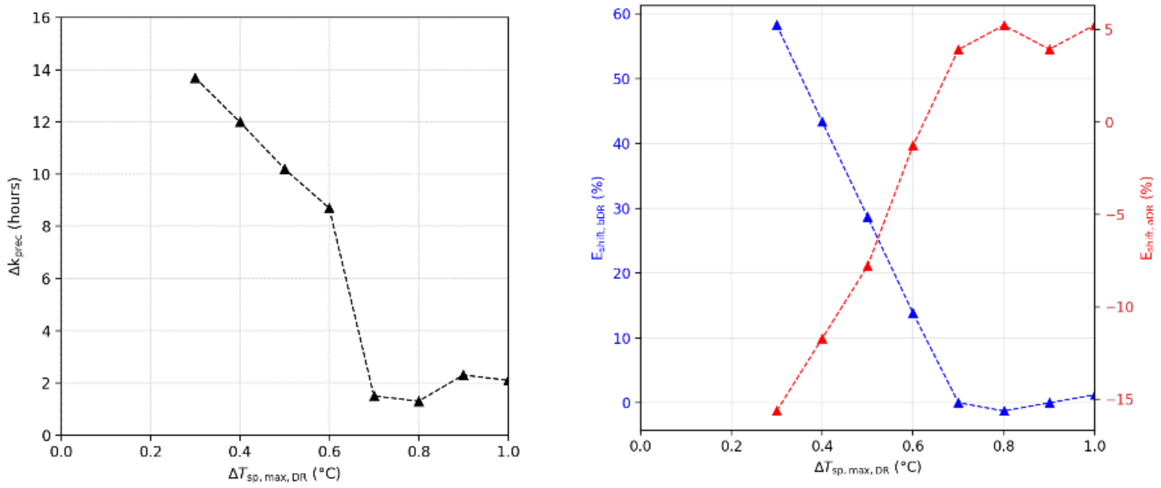

(a) (b)

Figure 8. Flexibility curves for split system with on-off regulation (f_{PSS} equal to 0, Δk_{DR} of 1 hour and $\Delta T_{sp,min,DR}$ equal to 2 °C): (a) Pre-cooling of the internal air node duration (Δk_{prec}) and (b) $E_{shift,bDR}$ and $E_{shift,aDR}$.

4.1.2 Fan coil Units (FCUs)

If a variable capacity heat pump coupled whit fan coil units is used to cover the cooling demand of the building, different electricity peak reductions can be obtained allowing a certain margin of flexibility to the indoor air temperature (T_{air}). In Figure 9(a) the same peak shaving event tested for the split system (Figure 7), in which a cancellation of the electricity peak (f_{PSS} equal to 0) is imposed for 1 hour (Δk_{DR} of 1 hour), is shown in comparison with the Baseline. In this case, the electricity peak is about 0.64 kW_{el} and it occurs at 2.00 pm. The flexibility range allows a lower band ($\Delta T_{sp,min,DR}$) of 2 °C and an upper band ($\Delta T_{sp,max,DR}$) of 0.5 °C.

In absence of thermal inertia, the flexibility provided by TCLs is exploited by means of a pre-cooling of about 6.25 hours and of a temperature rising (of 0.5 °C) during the event. Clearly, the extent of such flexibility exploitation depends on the possible temperature setpoints limits granted. However, due to the availability of such a single source of flexibility, not all the peak reductions can be realized (i.e., the optimization problem finds a feasible solution) and a great involvement of the temperature setpoints variation is generally required.

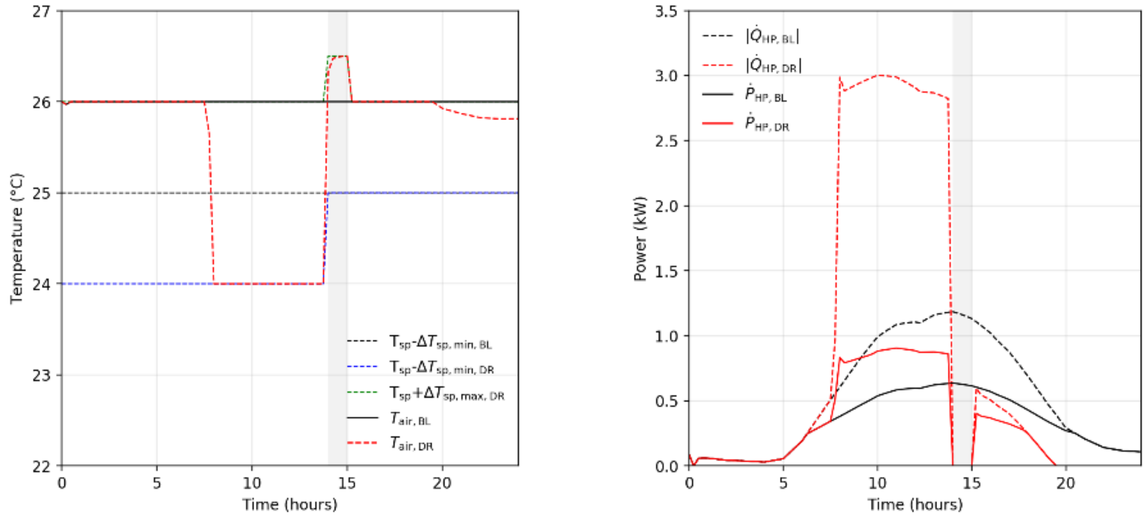

(a) (b)

Figure 9. Daily comparison between BL and DR event (f_{PSS} equal to 0, Δk_{DR} of 1 hour, $\Delta T_{sp,min,DR}$ of 2 °C, $\Delta T_{sp,max,DR}$ of 0.5 °C and $k_{start,DR}$ coinciding with $k_{peak,BL}$) for FCU without TES: (a) internal air node temperature and (b) thermal and electrical power of the heat pump.

In Figure 10 the flexibility curves to produce a 100 % reduction of the electricity consumption in 1 hour (Δk_{DR}) according to the different values of the upper and lower comfort bands (i.e. $\Delta T_{sp,max,DR}$ and $\Delta T_{sp,min,DR}$) are presented. It can be noticed that as the upper comfort band decreases, it also decreases the number of configurations in which the peak shaving can be realized. The results reported in Figure 10(a) highlight the role of the two comfort bands values ($\Delta T_{sp,max,DR}$ and $\Delta T_{sp,min,DR}$). In particular, if the upper comfort band assumes values between 0.9 °C and 1 °C, the event (f_{PSS} equal to 0 and Δk_{DR} of 1 hour) can be realized regardless of the values assumed by the lower comfort band, while on the other hand, only for the maximum value of the lower comfort band ($\Delta T_{sp,min,DR}$ equal to 2 °C) the event can be realized for each value greater than 0 °C of the upper comfort band. This behavior is also confirmed by the trend of $E_{shift,bDR}$ (Figure 10(b)). Indeed, for the higher values of the upper comfort band ($\Delta T_{sp,max,DR}$ from 0.8 °C to 1 °C) overconsumptions of less than 30 % are obtained (regardless of the value of the lower comfort band), on the other side, when high values of the lower comfort band ($\Delta T_{sp,min,DR}$) are allowed with low values of the upper comfort band ($\Delta T_{sp,max,DR}$), significant overconsumption must be expected ($E_{shift,bDR}$ greater than 40 % for $\Delta T_{sp,max,DR}$ lower than 0.6 ° C). However, the high involvement of the flexibility derived by TCLs in the hours before the peak reduction event positively affects the building response in the time after the event, as can be seen in Figure 10(c). Indeed, it can be noticed that as the $\Delta T_{sp,max,DR}$ decreases, regardless of the $\Delta T_{sp,min,DR}$, it increases the energy savings after the event ($E_{shift,aDR}$). This behavior suggests that the optimal solution evaluated to realize the event and to minimize the thermal demand aims to take advantage of the precooling also for the hours after the event.

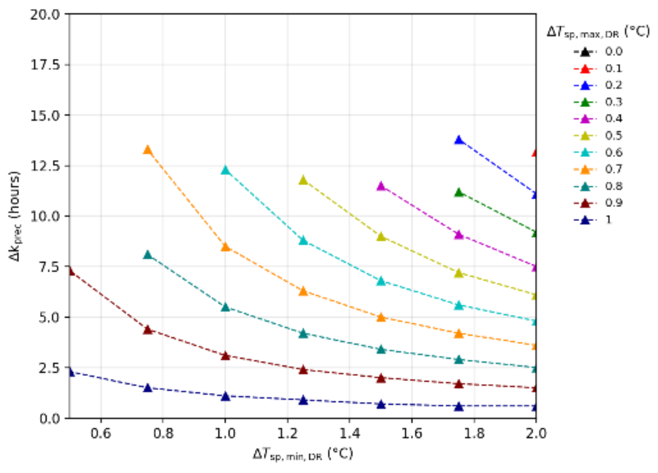

(a)

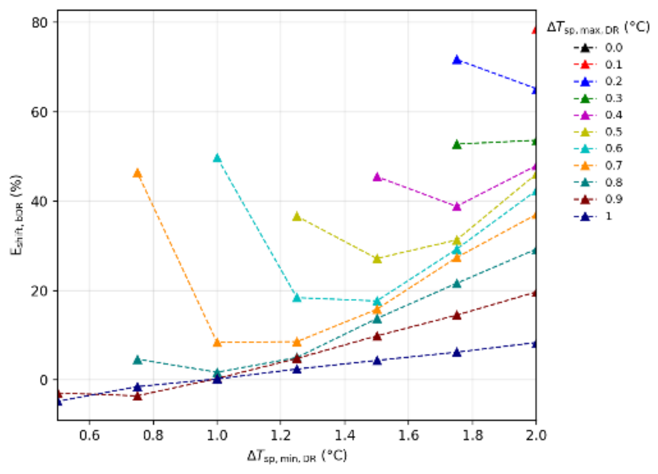

(b)

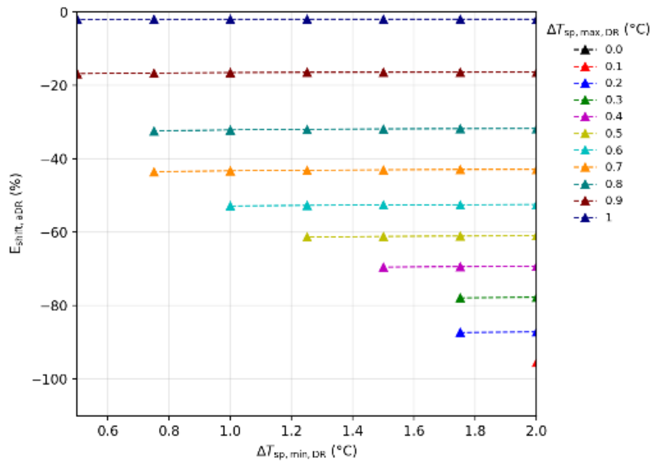

(c)

Figure 10. Daily flexibility curves for an event with f_{PSS} equal to 0 (100% peak reduction) and Δk_{DR} of 1 hour as the $\Delta T_{sp,max,DR}$ and $\Delta T_{sp,min,DR}$ vary for FCU (without TES): (a) Pre-cooling of the internal air node duration (Δk_{prec}), (b) $E_{shift,bDR}$ and (c) $E_{shift,aDR}$.

It is interesting to notice that, while for each value of the upper comfort band (for example $\Delta T_{sp,max,DR}$ equal to 0.7 °C) the duration of pre-cooling (Figure 10(a)) increases as the lower comfort band ($\Delta T_{sp,min,DR}$) decreases, $E_{shift,bDR}$ decreases with the lower comfort band (pre-cooling requires less heat to be removed). However, $E_{shift,bDR}$ reaches a minimum at a certain value of the lower comfort band (at $\Delta T_{sp,min,DR}$ of 1 °C for the curve relative to $\Delta T_{sp,max,DR}$ 0.7 °C in Figure 10(b)), then it starts to rise again. This is due to the fact that for small values of the lower comfort band

($\Delta T_{sp,min,DR}$ below 1 °C), very long pre-cooling times are required which greatly affect the electricity consumption. This behavior is confirmed by the curves in Figure 11: the thermal capacity of the heat pump decreases in power and increases in time when the lower comfort band decreases (Figure 11(c)). However, it is not translated in the same monotonous trend of the power ($\dot{P}^{*}_{shift}$ in Figure 11(b)) because of the nonlinear variation of the *EER* with the working conditions. In Figures 11(b) and (c) it can be also noticed the lowering of the electrical and the thermal demand in the hours after the event that can be obtained thanks to the exploitation of the pre-cooling.

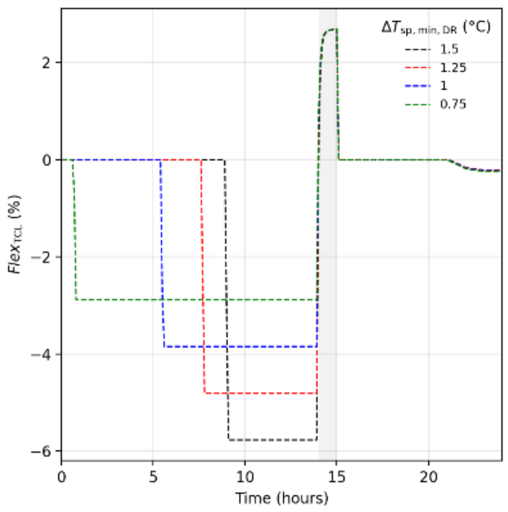

(a)

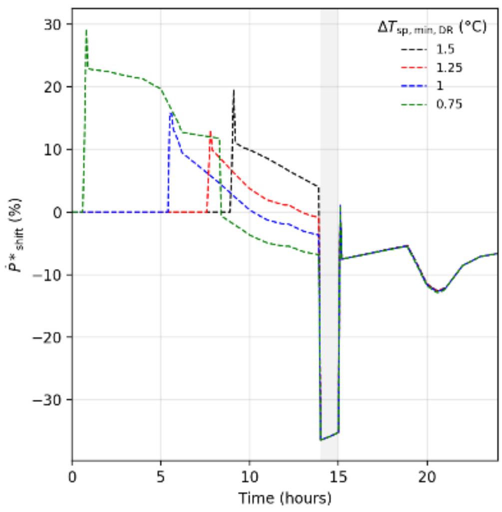

(b)

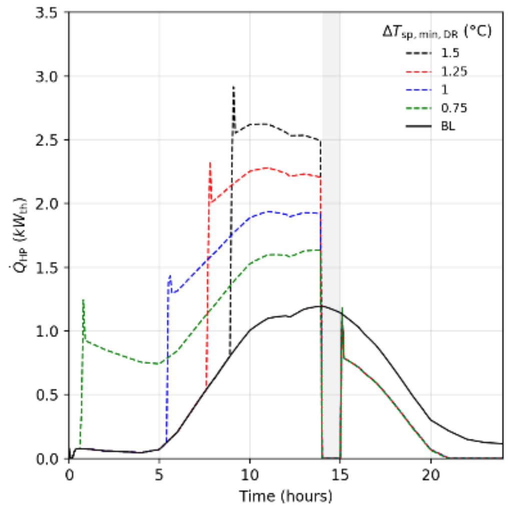

(c)

Figure 11. Daily Demand Response operation (f_{PSS} equal to 0, Δk_{DR} of 1 hour, $\Delta T_{sp,max,DR}$ of 0.7 °C and with variable $\Delta T_{sp,min,DR}$) for FCU (without TES): (a) $Flex_{TCL}$, (b) $\dot{P}^{*}_{shift}$ and (c) thermal power of the HP.

In APPENDIX A the flexibility curves with different peak reductions are reported. As expected, the flexible behavior of the system is the same as discussed for the previous case (f_{PSS} equal to 0) with a scaled trend (i.e., as the peak reduction decreases both the duration of the pre-cooling phase, Δk_{prec}, and the electricity consumption variation before the event, $E_{sfhit,bDR}$, decrease, while the electricity saving after it, $E_{sfhit,aDR}$, increases). In any case, in all the tested configurations of peak shaving (see APPENDIX A) it is clear that, a high involvement of the user (in term of setpoint variations) has to be taken into account when no thermal inertia is available, especially to produce high electricity consumption reductions. Anyhow, if a large variation of the setpoint is allowed during the event (minimum $\Delta T_{sp,max,DR}$

of 1 °C), the system, due to the rapidity of the variation, allows to realize all the required consumption reductions, with low values of pre-cooling time (lower than 2.25 hours).

Hence, it is possible to conclude that when there is no thermal inertia, the possible demand variation produced by exploiting the TCLs is limited and, where possible, it consistently affects the users comfort conditions. On the contrary, if a TES is added to the water circuit of the fan coil, its thermal inertia allows to realize different types of Demand Response events even without setpoint temperature modifications. In Figure 12 the same peak reduction of Figures 7 and 9 realized in the configuration with the TES is shown. In this case the flexibility from TCLs before the event is not exploited (Δk_{prec} is equal to 0 hours) and the cooling power stored in the TES is used during the event (Figure 12(b)). Moreover, also a lower $E_{shift,bDR}$ is calculated. It is + 23 % in case of FCU with TES in comparison to + 46 % in the configuration without the TES.

In order to highlight the role of the TES, Figure 13 represents the comparison between the flexibility evaluation parameters ($Flex_{TCL}$ and $\dot{P}^{*}_{shift}$) for the FCU system with and without the presence of the TES: also considering the most extreme case treated ($\Delta T_{sp,min,DR}$ equal to 0.5 °C and $\Delta T_{sp,max,DR}$ equal to 0 °C), a $Flex_{TCL}$ of 0 % is calculated throughout the day (Δk_{prec} of 0 hours) in presence of TES.

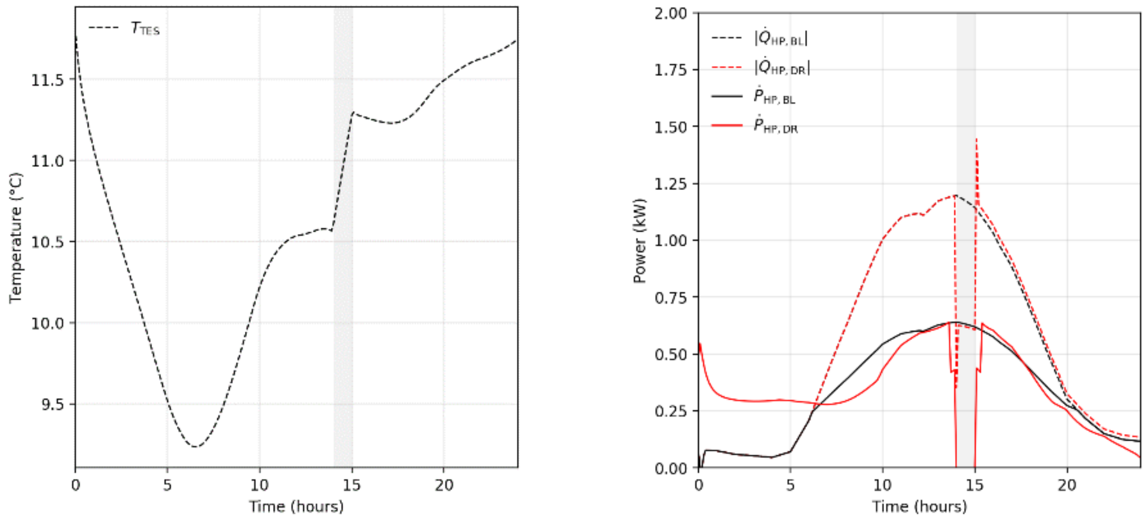

(a) (b)

Figure 12. Daily comparison between BL and DR event (f_{PSS} equal to 0, Δk_{DR} of 1 hour, $\Delta T_{sp,min,DR}$ of 2 °C, $\Delta T_{sp,max,DR}$ of 0.5 °C and $k_{start,DR}$ coinciding with $k_{peak,BL}$) for FCU with TES: (a) TES node temperature and (b) thermal and electrical power of the heat pump.

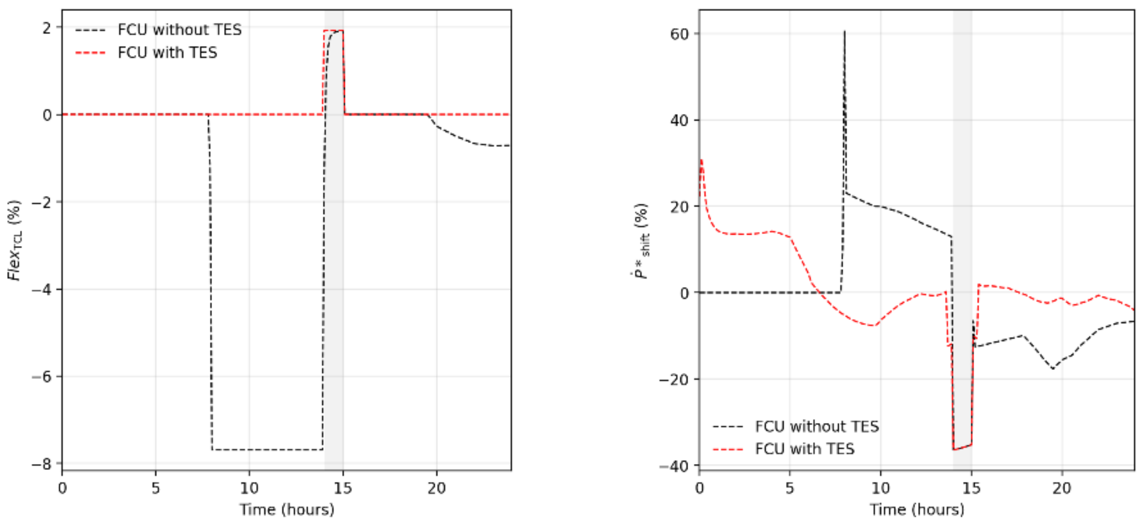

(a) (b)

Figure 13. Daily Demand Response operation (f_{PSS} equal to 0, Δk_{DR} of 1 hour, $\Delta T_{sp,min,DR}$ of 2 °C, $\Delta T_{sp,max,DR}$ of 0.5 °C and $k_{start,DR}$ coinciding with $k_{peak,BL}$) for FCU with and without TES: (a) $Flex_{TCL}$ and (b) $\dot{P}^{*}_{\text{shift}}$.

Looking at Figure 5 it can be noticed that the charging of the TES in the hours before the event (Figure 14(a)) produces an average increase of +22.7 % in the electricity consumption in the hours before the event while the average electricity saving after it is -15.9 % ($E_{shift,bDR}$ and $E_{shift,aDR}$ in Figure 15). The increase in the electricity demand can be observed also in Figure 14(b), where $\dot{P}^{*}_{\text{shift}}$ is represented.

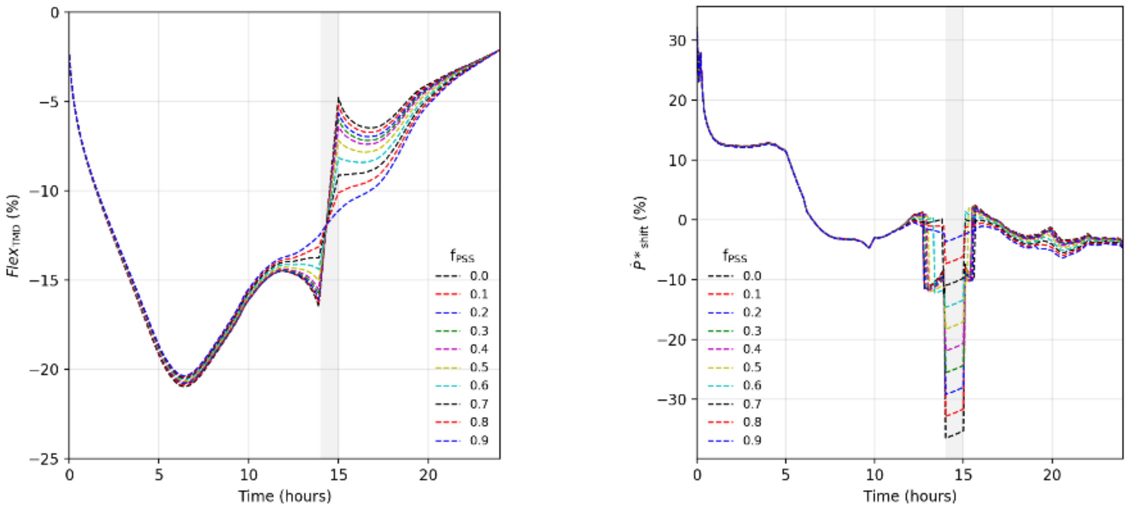

(a) (b)

Figure 14. Daily Demand Response operation (Δk_{DR} of 1 hour, $\Delta T_{sp,max,DR}$ of 0 °C and $\Delta T_{sp,min,DR}$ of 0.5 °C) for FCU with TES as the f_{PSS} varies: (a) $Flex_{TMD}$ and (b) $\dot{P}^{*}_{\text{shift}}$.

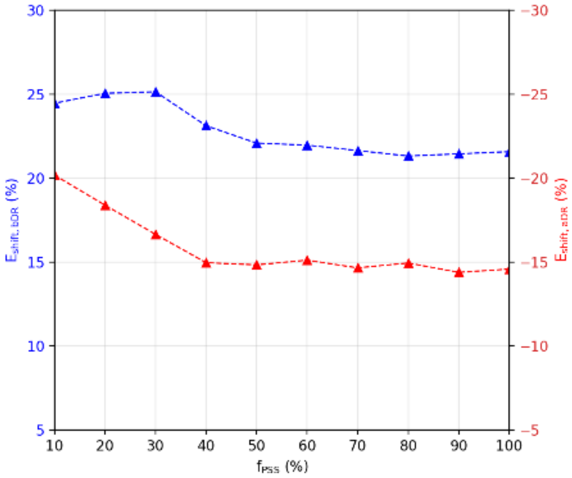

Figure 15. Daily flexibility curve related to $E_{shift,bDR}$ and $E_{shift,aDR}$ (Δk_{DR} of 1 hour, $\Delta T_{sp,max,DR}$ of 0 °C and $\Delta T_{sp,min,DR}$ of 0.5 °C) for FCU with TES as the f_{PSS} varies.

On the basis of these results it is therefore possible to conclude that, for the FCU system, the only way to produce different events without involving the end user's thermostat is to provide a thermal storage system (i.e., FCU with TES). Indeed, if the TES is added to the FCU distribution system, its thermal mass contribution (the temperature T_{TES} represents the temperature of the TMD) allows to implement all the peaks reduction so far discussed without any involvement of the air node setpoint temperature.

4.1.3 Ceiling panels (CP) with dehumidifier (DH)

In the ceiling panels system (CP) the sensible cooling power provided by the heat pump is not removed directly from T_{air} but it is provided to the inner layer of the roof ($T_{ri,cp}$ in Figure 3). From this decoupling, a minimum level of thermal inertia can be derived by the mass of the envelope and the system is able to realize differently the peak shaving events with also minimum variations of the comfort bands (i.e., $\Delta T_{sp,min,DR}$ and $\Delta T_{sp,max,DR}$).

Focusing on an event that imposes a 100 % peak reduction (f_{PSS} equal to 0), in the same conditions tested in the previous sections (Δk_{DR} of 1 hour, $\Delta T_{sp,min,DR}$ of 2 °C, $\Delta T_{sp,max,DR}$ of 0.5 °C and $k_{start,DR}$ coinciding with $k_{peak,BL}$), the comparison between the Demand Response event and the Baseline is shown in Figure 16.

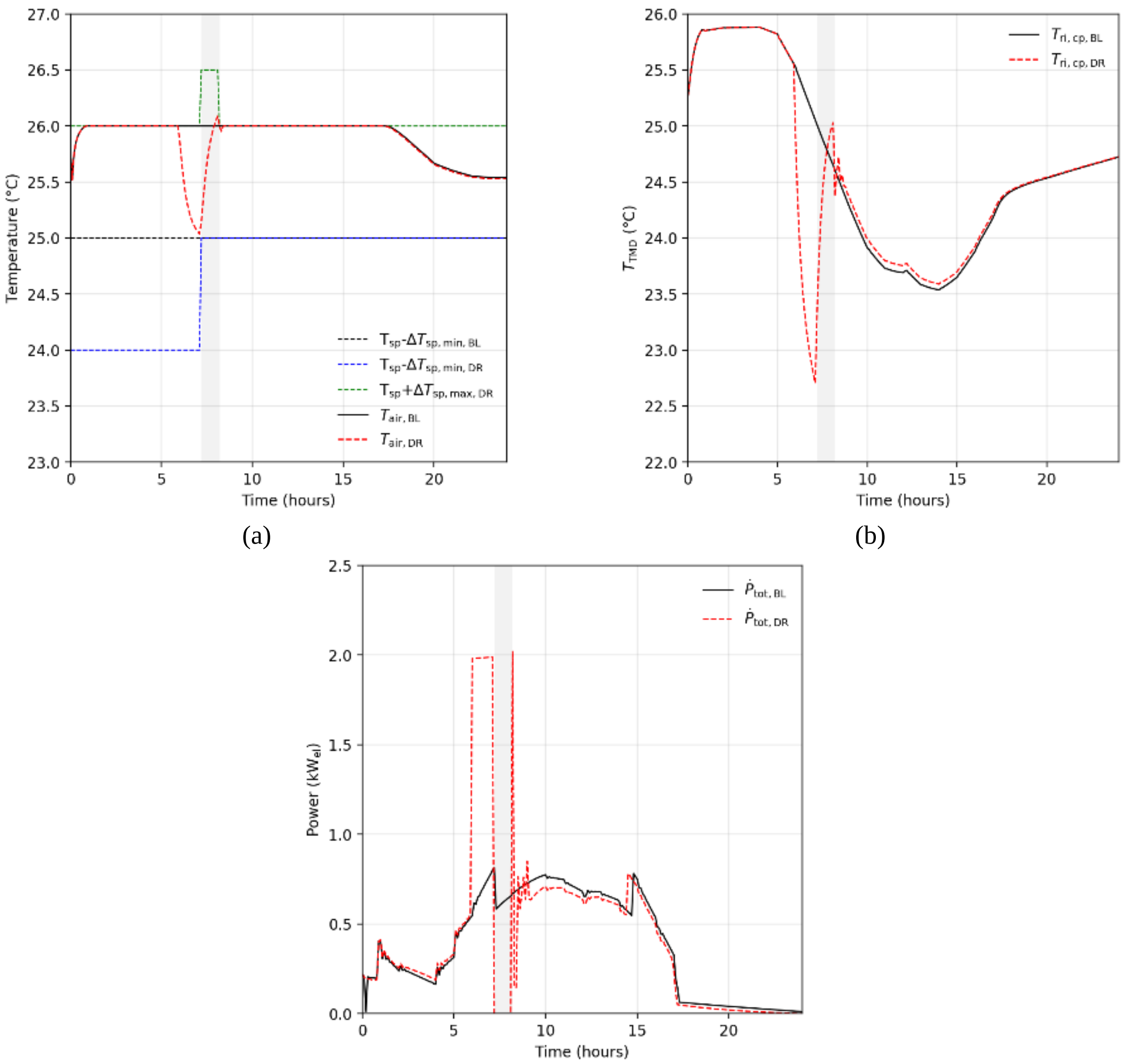

(a) (b)

(c)

Figure 16. Daily comparison between BL and DR event (f_{PSS} equal to 0, Δk_{DR} of 1 hour, $\Delta T_{sp,min,DR}$ of 2 °C, $\Delta T_{sp,max,DR}$ of 0.5 °C, $\Delta RH_{sp,min,DR}$ of 5 %, $\Delta RH_{sp,max,DR}$ of 5 % and $k_{start,DR}$ coinciding with $k_{peak,BL}$) for CP: (a) air node; (b) roof node temperatures and (c) electrical consumption (HP and DH).

In this case, since the cooling system is also equipped with a dehumidifier to control the indoor relative humidity, the electricity peak time is estimated on the total electricity consumption curve (DH and HP). In particular the peak (in Baseline) occurs at 7.20 am with a value of 0.82 kW_{el} (of which 14.6 % is derived from the dehumidifier and the remaining 85.4 % from the heat pump). The total electricity consumption is 9.2 kWh_{el}, 75 % of that is produced by the HP and the remaining 25 % by the DH.

Looking at the red curves in Figures 16(a) and (b) which represent the results of the Demand Response event, it can be noted that, thanks to the thermal mass of the roof layer, the CP system allows a low exploitation of TCLs. Indeed, the pre-cooling is about 1.2 hours. However, to cool down $T_{ri,cp}$, the anticipated overconsumption of the heat pump is significantly higher (Figure 16(c)) with a $E_{shift,bDR}$ of 67 % (the $\dot{P}^{*}_{shift}$ curve (Figure 17(b)) reaches values of 72 % during the precooling phase). Figure 17(a) shows the dynamic involvement of each energy flexibility source (i.e. flexibility of the thermostatically controlled loads, thermal mass and relative humidity variation) for the tested event. In particular, for the relative humidity flexibility parameter ($Flex_{RH}$), it can be noted that during the peak shaving event, $Flex_{RH}$ decreases while it increases in the preceding hours. However, this is not derived by an optimized control logic, but it is a simple consequence of the internal temperature trend (T_{air}). Therefore, the flexibility linked to the variation of the relative humidity is strictly dependent on the temperature variation.

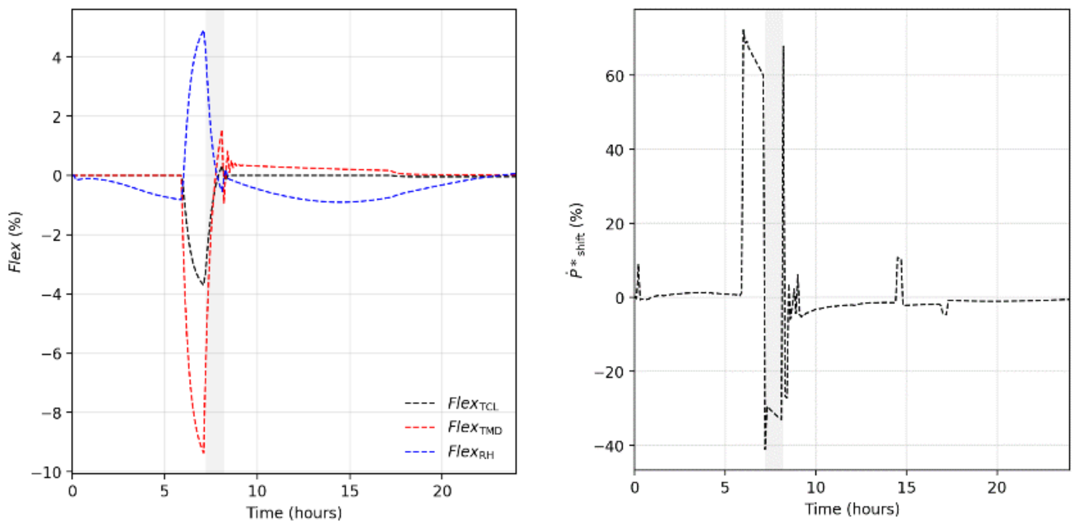

(a) (b)

Figure 17. Daily Demand Response operation (f_{PSS} equal to 0, Δk_{DR} of 1 hour, $\Delta T_{sp,min,DR}$ of 2 °C, $\Delta T_{sp,max,DR}$ of 0.5 °C, $\Delta RH_{sp,min,DR}$ of 5 %, $\Delta RH_{sp,max,DR}$ of 5 % and $k_{start,DR}$ coinciding with $k_{peak,BL}$) for CP: (a) $Flex_{TCL}$, $Flex_{TMD}$ and $Flex_{RH}$ and (b) $\dot{P}^{*}_{shift}$.

Thanks to the involvement of both the TMD and the TCLs in the ceiling panels system, the configurations in which the events are not feasible decrease considerably. As showed in the flexibility curves of Figure 18, in which a peak annulment (f_{PSS} of 0 for 1 hour) is tested in different conditions of temperature setpoint limits, the optimization problem finds a feasible solution for each combination of the comfort bands ($\Delta T_{sp,max,DR}$ and $\Delta T_{sp,min,DR}$). However, focusing on the cases shown in Figure 18, a lower influence of the comfort limits on the realization of the event in CP may be noted. In particular, only the lowest values of the comfort bands ($\Delta T_{sp,min,DR}$ under 1 °C) produce a worsening of performance in term of Δk_{prec} (Figure 18(a)).

In the other cases ($\Delta T_{sp,min,DR}$ greater than 1 °C), similar values of Δk_{prec} and $E_{shift,bDR}$ are calculated regardless the values assumed by the comfort limits. Looking at Figure 18(c) it can be noticed that, also in this case the pre-cooling allows to produce a lowering of the electricity demand also in the hours after the event.

Moreover, no influence of the parameter $\Delta RH_{sp,max,DR}$ and $\Delta RH_{sp,min,DR}$ is observed (APPENDIX B).

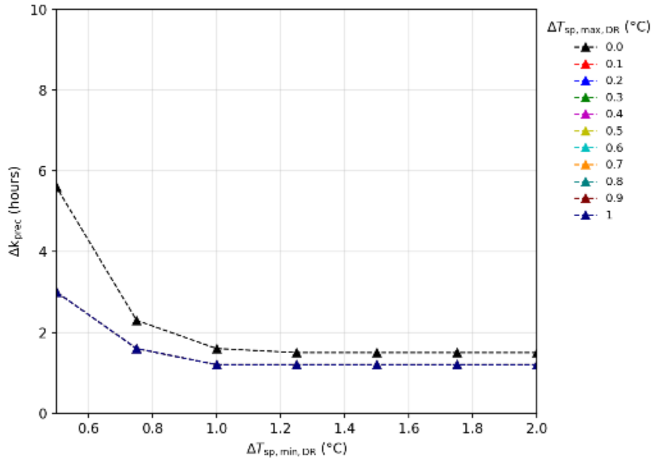

(a)

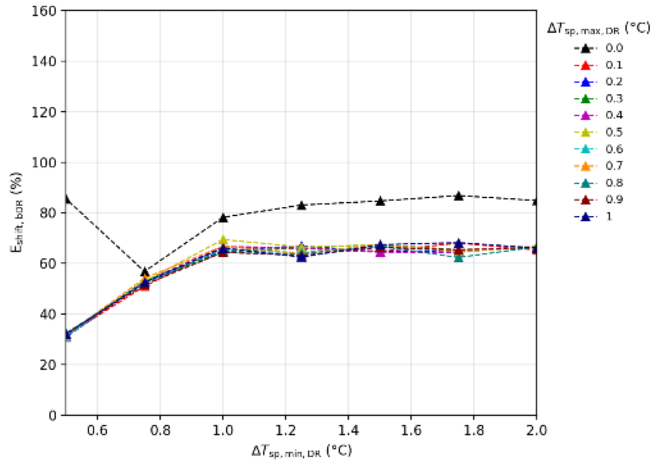

(b)

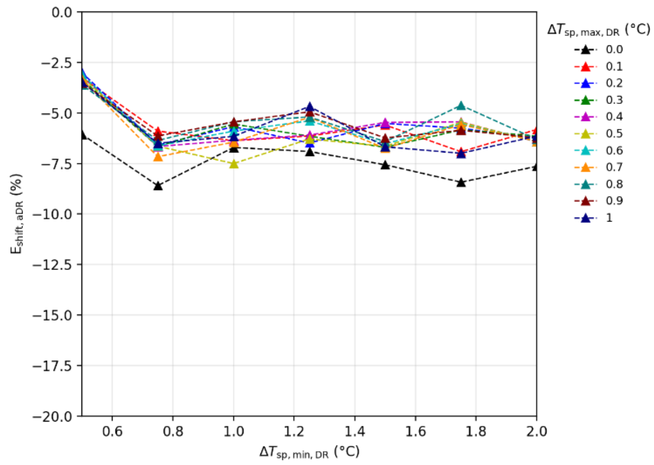

(c)

Figure 18. Daily flexibility curves for an event with f_{PSS} equal to 0 (100% peak reduction) and Δk_{DR} of 1 hour as the $\Delta T_{sp,max,DR}$ and $\Delta T_{sp,min,DR}$ vary for CP ($\Delta RH_{sp,min,DR}$ and $\Delta RH_{sp,max,DR}$ equal to 5 %): (a) Pre-cooling of the internal air node duration (Δk_{prec}), (b) $E_{shift,bDR}$ and (c) $E_{shift,aDR}$.

In Figure 19, the dynamic comparison between the case in which the 100 % peak reduction is produced with the lowest and the greatest values of the upper comfort band ($\Delta T_{sp,max,DR}$ respectively 0 °C and 1°C) with a fixed values of 1 °C for the lower comfort band $\Delta T_{sp,min,DR}$ is shown. Looking at Figure 19(d) it can be immediately noted the high peak values reached by the $\dot{P}^{*}_{shift}$ curves (near 80%) in the time before the event in both configurations. In particular, in case of upper comfort band ($\Delta T_{\mathrm{sp,max,DR}}$) equal to 1 °C (red curves in Figure 19) also a peak in the $\dot{P}^{*}_{\mathrm{shift}}$ after the event occurs although the overall consumption decreases in the hours following the event ($E_{\mathrm{shift,aDR}}$ in Figure 18(c)). Moreover, due to the storage capability of the ceiling panels and its slower speed in following precise variations in the internal temperature (heat is not removed directly from T_{air}), even with a $\Delta T_{\mathrm{sp,max,DR}}$ of 1 °C, the internal temperature takes the entire duration of the event (Δk_{DR}) to rise (Figure 19(a)) up to 26.1 °C (not all the allowed $\Delta T_{\mathrm{sp,max,DR}}$ is exploited). Looking at Figure 19(b), a variation of $Flex_{\mathrm{RH}}$ can be appreciated. However, as mentioned, it is only a consequence of the sensitive cooling of the internal air in the precooling. In Figure 19(c) instead, the utilization of the flexibility of the thermal mass of the distribution system ($Flex_{\mathrm{TMD}}$) is represented. Because of the low thermal inertia of the $T_{\mathrm{ri,cp}}$ node, the latter has the same trend of $Flex_{\mathrm{TCL}}$ However, $Flex_{\mathrm{TMD}}$ reaches twice as low values as during the pre-cooling phase. This is the reason why high overconsumption are evaluated (Figures 18(b) and 19(d)). Similar behaviors can be observed for lower peak reductions (f_{PSS} greater than 0) as showed in APPENDIX B.

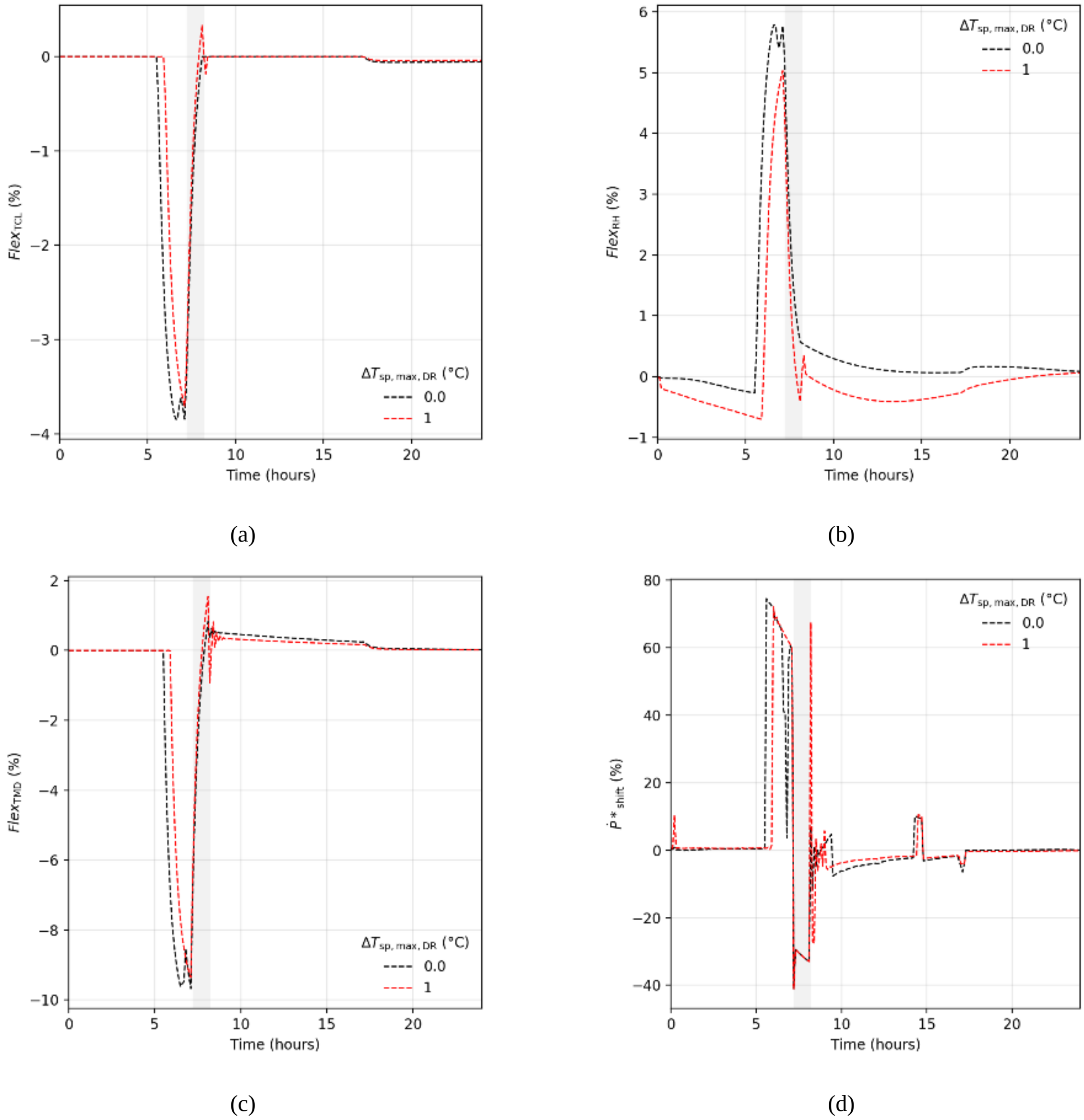

Figure 19. Daily Demand Response operation (f_{PSS} equal to 0, Δk_{DR} of 1 hour, $\Delta T_{\mathrm{sp,max,DR}}$ of 0 °C and 1 °C and $\Delta T_{\mathrm{sp,min,DR}}$ of 1 °C) for CP: (a) $Flex_{\mathrm{TCL}}$, (b) $Flex_{\mathrm{RH}}$, (c) $Flex_{\mathrm{TMD}}$ and (c) $\dot{P}^{*}_{\mathrm{shift}}$.

4.1.4 Cooling concrete ceiling (CC) with dehumidifier (DH)

When the cooling power of the heat pump is removed from a high massive node, as in case of concrete ceiling cooling system (CC), the Demand Response event analyzed for the previous cases (f_{PSS} equal to 0 for Δk_{DR} of 1 hour) can be implemented with a low involvement of the TCLs flexibility. Indeed, the high storage capability of the roof node (T_{ri} in Figure 2) allows to keep the air temperature near to the setpoint of 26 °C (Figure 20(a)) during the event at the expense of a pre-cooling of the thermal mass of the distribution system (Figure 20(b)).

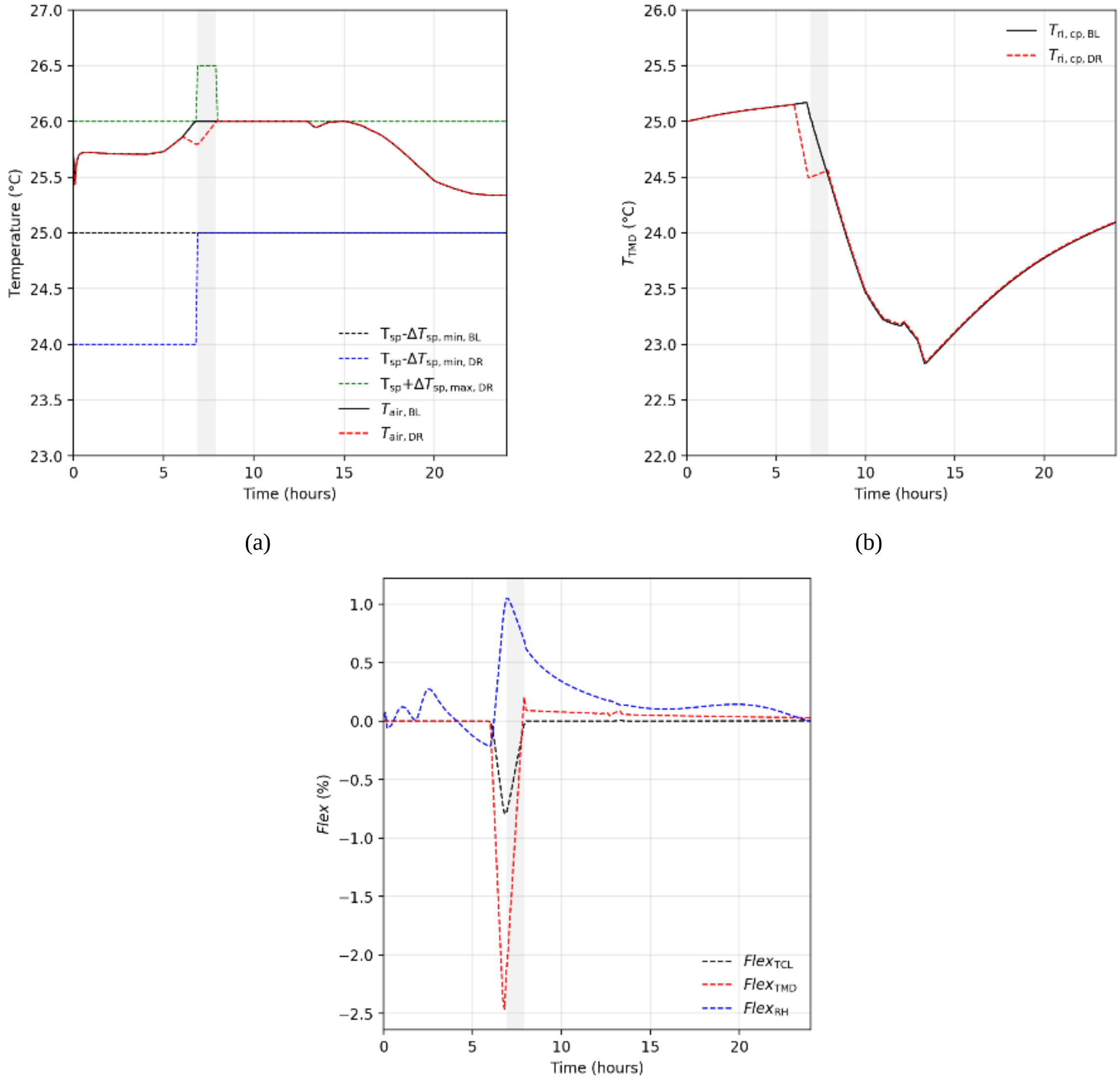

(a) (b) (c)

Figure 20. Daily Demand Response operation (f_{PSS} equal to 0, Δk_{DR} of 1 hour, $\Delta T_{sp,min,DR}$ of 2 °C, $\Delta T_{sp,max,DR}$ of 0.5 °C, $\Delta RH_{sp,min,DR}$ of 5 %, $\Delta RH_{sp,max,DR}$ of 5 % and $k_{start,DR}$ coinciding with $k_{peak,BL}$) for CC: (a) air node temperature, (b) roof node temperature and (c) $Flex_{TCL}$, $Flex_{TMD}$ and $Flex_{RH}$.

Although the variation of the temperature of the thermal mass node (T_{ri}) is relatively small ($Flex_{TMD}$ reaches the minimum value of - 2.5 % in Figure 20(c)), the large thermal inertia of the cooling system involves a not negligible increase in the power curve (Figure 21). Indeed, due to the high involvement of the thermal inertia of the distribution system, the estimated increase of electricity consumption before the peak shaving event becomes 116 % ($E_{shift,bDR}$) with a peak of almost 100 % in the $\dot{P}^{*}_{shift}$ curve (Figure 21(b)). In this case, also the electricity consumption after the event increases (1.24 % of $E_{shift,aDR}$). Indeed, a peak power can be observed even immediately after the event (Figure 21).

It is important to highlight that in this case, as for CP, also the relative humidity is controlled by the cooling system with a dehumidifier and the power curves showed in Figures 21(a) and (b) take into account both contributions. The trend of the parameter $Flex_{RH}$ (Figure 20(c)) shows again its dependence on the temperature, which has a prevalent impact on the achievement of the comfort limits.

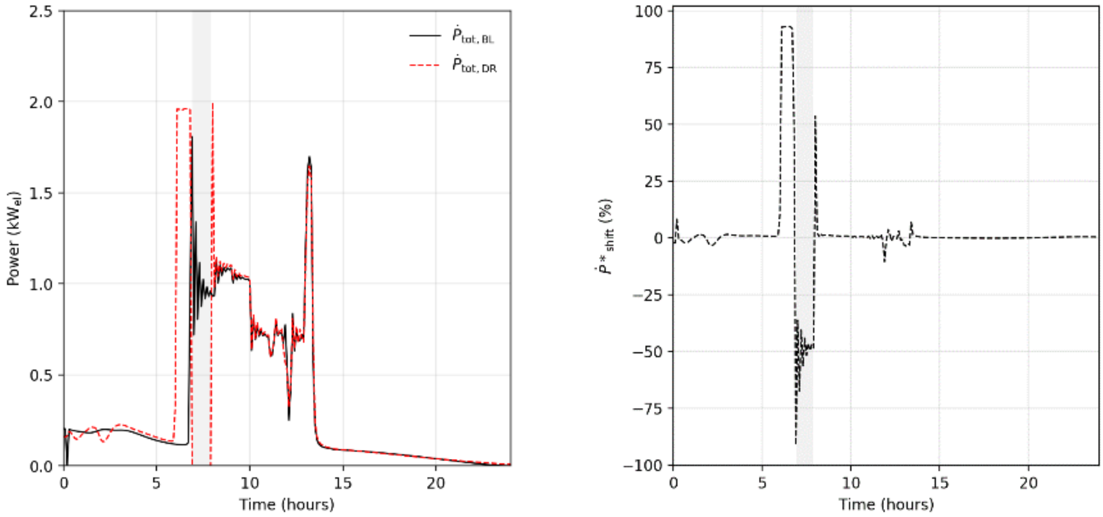

(a) (b)

Figure 21. Daily Demand Response operation (f_{PSS} equal to 0, Δk_{DR} of 1 hour, $\Delta T_{sp,min,DR}$ of 2 °C, $\Delta T_{sp,max,DR}$ of 0.5 °C, $\Delta RH_{sp,min,DR}$ of 5 %, $\Delta RH_{sp,max,DR}$) for CC: (a) electrical consumption (HP and DH) and (b) $\dot{P}^{*}_{shift}$.

In Figure 22, the flexibility curves in case of 100 % peak reduction in different conditions of comfort bands are showed, while Figure 23 represents the dynamic flexible behavior in the same cases with a focus on a fixed value of the lower comfort band ($\Delta T_{sp,min,DR}$ equal to 1 °C).

Looking at Figure 23(a) it can be noted that during the event the upper comfort range ($\Delta T_{sp,max,DR}$) is not exploited and $Flex_{TCL}$ does not reach the value - 1 % in the time before the event. Therefore, albeit a precooling time of 0.6 hours (Δk_{prec} in Figure 22(a)) is measured, it does not correspond to an effective exploitation of the lower flexibility band ($\Delta T_{sp,min,DR}$). On the contrary, considering the large thermal mass of the CC system, the flexibility of the thermal mass of the distribution system is more involved ($Flex_{TMD}$ reaches the value of - 2.5 %, Figure 23(c)). This is also the reason why a higher increase in the electricity power consumption is obtained (Figures 22(b) and 23(d)). It is interesting to notice that, when a large thermal inertia is involved to realize the event, even a delayed power peak after the event is always observed (Figure 23(d)) and the electricity consumption after the event is always greater than 0 % (Figures 22(c)).

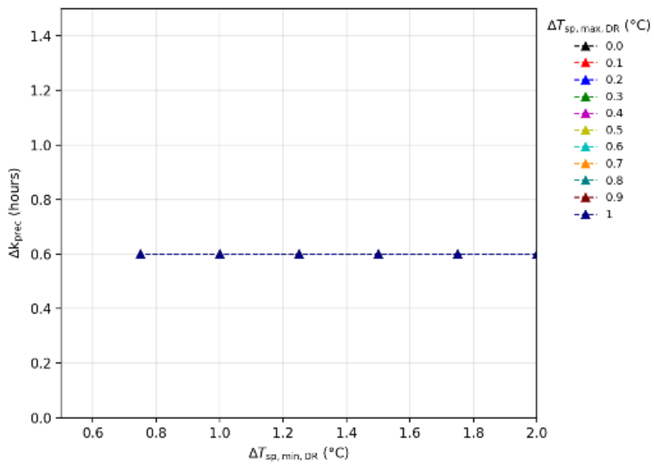

(a)

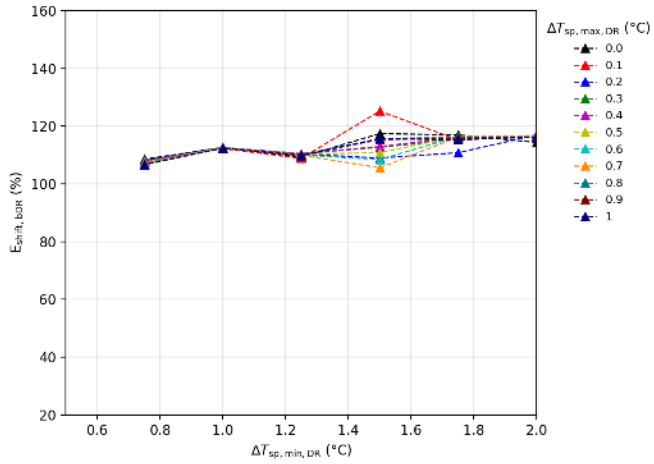

(b)

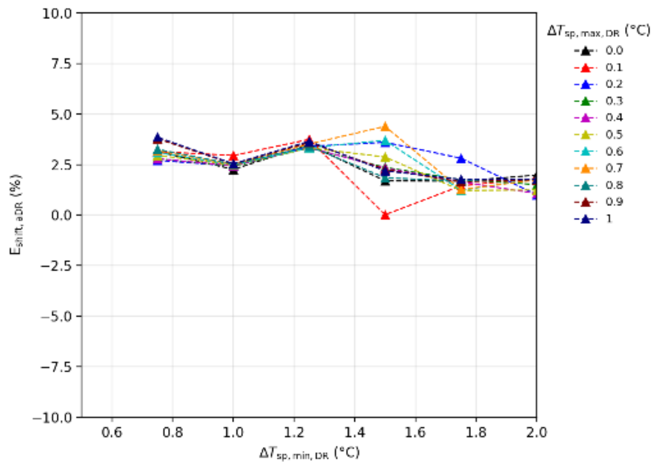

(c)

Figure 22. Daily flexibility curves for an event with f_{PSS} equal to 0 (100 % peak reduction) and Δk_{DR} of 1 hour as the $\Delta T_{sp,max,DR}$ and $\Delta T_{sp,min,DR}$ vary for CC ($\Delta RH_{sp,min,DR}$ and $\Delta RH_{sp,max,DR}$ equal to 5 %): (a) Pre-cooling of the internal air node duration (Δk_{prec}), (b) $E_{shift,bDR.}$ and (c) $E_{shift,aDR}$.

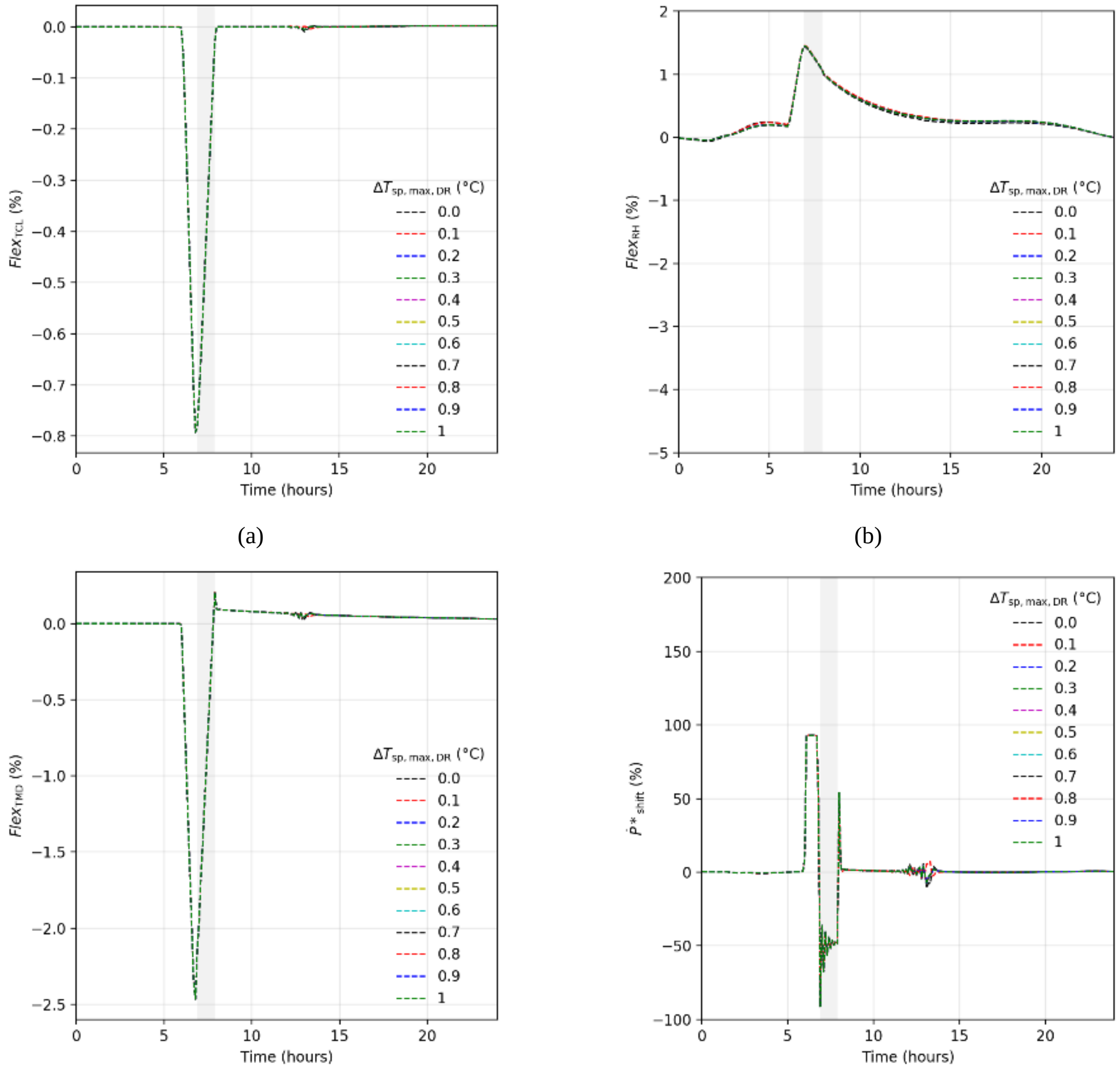

(a) (b) (c) (d)

Figure 23. Daily Demand Response operation (f_{PSS} equal to 0, Δk_{DR} of 1 hour, $\Delta T_{sp,max,DR}$ varies and $\Delta T_{sp,min,DR}$ of 1 °C) for CC: (a) $Flex_{TCL}$, (b) $Flex_{RH}$, (c) $Flex_{TMD}$ and (c) $\dot{P}^{*}_{shift}$.

More flexibility curves about the CC systems are reported in APPENDIX C, where a focus on different peak reductions values is also provided. Looking at the flexibility curves reported in APPENDIX C, it can be noted that the behavior of the cooling concrete ceiling plant (CC) in producing a certain peak reduction is quite independent on the Demand Response parameters. This is due to the fact that, the storage capacity of the distribution system (TMD) is mostly used. In particular, it is interesting to notice that for peak reductions lower that 60 %, the CC system allows to avoid almost entirely the involvement of the flexibility derived by TCLs regardless of the values assumed by limits granted to the thermostat.

To conclude, it is possible to observe that when the heat is accumulated in a high massive layer of the building envelope (e.g., the roof), different peak shaving events can be performed thus limiting the effect on the indoor temperature to a minimum. On the contrary, large over energy consumption are expected, both before and after the event.

4.2 Comparison between the Space Cooling systems

The presented analysis demonstrates that Space Cooling technologies differ in terms of type and entity of exploitation of different flexibility resources (i.e. the involvement (i) of the thermostatic controlled loads or (ii) of the thermal inertia of the distribution system) with different consequences on the electric power curve (i.e. presence of payback loads) during peak shaving events.

As far as the split systems are concerned, they are the most inflexible systems among those analyzed. Indeed, as it does not allow any modulation of the heat pump, the split can realize only a Demand Response event with a reduction factor (f_{PSS}) equal to zero. Moreover, a high involvement of the user's temperature setpoint is necessary, not having any thermal inertia available. Another important aspect that can be noticed by observing the split power curves (Figure 7) involves the difficulty in predicting the trend of the electricity demand in the period before and after the event. This last point, due to the cycling of the heat pump, differentiates the behavior of this technology (on-off regulation) from all the other systems modeled. In fact, all the other emission systems (i.e. FCU, CC and CP) are equipped with a variable capacity heat pump which allows a modulation of the load.

The fan coil, in its configuration without the TES, as for the split, requires a high involvement of the TCLs (Figure 10(a)) because there is no thermal inertia. However, thanks to the load modulation, the FCU can realize a larger number of peak reductions than the split system, even if, as for the SS, the peak power annulment cannot be obtained for each comfort band. Moreover, the variable capacity heat pump affects also the way in which the event is produced. In other words, the limits granted to the setpoint have a great impact in the implementation of the event both in the period before, during and after it. Indeed, if a large variation of the setpoint is allowed during the event (minimum $\Delta T_{sp,max,DR}$ of 1 °C, Figure 10(a)), the FCU, due to its rapidity, can realize all the required consumption reductions with short pre-cooling (lower than 2.25 hours) and low electricity overconsumptions before the event, ($E_{sfhift,bDR}$ lower than 10 % in Figure 10(b)).

A reduced involvement of the user's temperature setpoints can be achieved if a thermal energy storage is added to the fan coil water circuit. In fact, in this case, the exploitation of the thermal inertia of the distribution system produces any peak reductions without modifying the temperature setpoint of the users. This is due to the complete decoupling of demand from generation possible thanks to the storage device added to the plant. On the other hand, although reductions in electrical absorption are achieved after the event (Figure 15), overconsumption must be expected in the moments preceding the event due to the tank charging phase (Figure 15).

Therefore, it clearly appears that, even just considering these three types of emission systems (i.e. SS, FCU with and without TES) when the thermal mass available in the thermal distribution system increases, the involvement of the flexibility from TCLs decreases. This behavior is also confirmed by the observation of the results obtained for the massive ceiling systems (i.e. CP and CC). Referring to the same Demand Response event, it can be noted that, thanks to the thermal mass of the roof layer, the CP system requests a lower exploitation of TCLs than the case of the FCU system without the TES both during and before the event. Furthermore, the pre-cooling in the CP is about 81% shorter than the case of FCU. However, to cool down the roof layer of the CP system, the anticipated overconsumption of the heat pump is significantly high ($E_{shift,bDR}$ of + 67 % in case of CP while it is 46 % in case of FCU): $E_{shift,bDR}$ of the CP system is due to a higher electricity power involvement for a shorter period (as showed in Figure 17(b), the $\dot{P}^{*}_{\text{shift}}$ curve reaches values of 72 % during the precooling phase). Nevertheless, albeit to a lesser extent than the FCU without TES (Figure 18(a) in comparison to Figure 10(a)), a certain influence of the comfort limits modification can be observed also on CP systems, because their thermal inertia is limited. On the other hand, the same behavior is not observed for the electricity overconsumption. Indeed, while for the FCU without TES the high involvement of the users' setpoint allows to avoid payback loads, the exploitation of the thermal mass of the CP system does not avoid this effect, regardless of the comfort limits granted (Figure 10(b) in comparison to Figure 18(b)). In particular, for some values of upper comfort band ($\Delta T_{\mathrm{sp,max,DR}}$ equal to 1 °C in Figure 19(d)) in the CP system also a peak in the $\dot{P}^{*}_{\mathrm{shift}}$ after the event occurs.

To summarize two important aspects can be highlighted.

- First of all, although with ceiling panels the pre-cooling times are generally lower than in the previous cases (SS and FCU without TES), there is no configuration that allows to carry out a complete reduction of the peak with a pre-cooling lower than 1 hour, which instead happens in the FCU (configuration with the TES or with a high exploitation of the flexibility from TCL).
- Moreover, especially for the most extreme peak reduction (f_{PSS} equal to 0, 0.1 and 0.2 in APPENDIX B), there is always an increase in electricity consumed before the event ($E_{\mathrm{shift,bDR}}$ greater than 0 %), while in the case of FCU it can be almost zero with high involvement of the flexibility from TCLs (APPENDIX A).

This difference between these two systems is emphasized when, instead of the CP, a high massive cooling system (i.e. CC) is considered. From the results obtained for concrete ceiling cooling system, it appears that as the thermal inertia level of the node from which the heat is removed increases, the realization of different peak shaving events is possible with the minimum involvement of the flexibility from TCLs. Furthermore, the way in which the events are implemented is almost completely independent on the limits granted to the temperature setpoint (Figure 22). This behavior is similar to that obtained for the FCU in the configuration with TES, even if an important difference in terms of electrical overconsumption and payback loads can be observed between the two systems. The exploitation of a high massive cooling system produces important consequences on the electric power curve both before and after the event. Moreover, even with high levels of thermal mass in the ceiling (as for the CC), a complete decoupling of demand from generation is not possible, thus it is never possible to completely avoid the involvement of users when a peak annulment is required, as it happens with the TES added to the FCU. This aspect must therefore be considered when planning a load management strategy with this type of systems.

5. CONCLUSIONS

Objective of this work was to evaluate qualitatively and quantitatively the operational energy flexibility of the residential space cooling demand. While modelling several technologies (split systems, fan coils with and without TES, ceiling panels, concrete ceiling), attention was paid to the role of the thermal emission systems in the load shifting capability. The systems analyzed represent the most common technologies and are characterized by different sources of flexibility, i.e. the thermal inertial of the system itself or the flexibility provided by the variation of the indoor temperature setpoint (thermostatically controlled loads). In the evaluation, several Demand Response events (i.e., peak shaving strategies) have been tested in comparison with a reference scenario (Baseline). The flexibility potential of each cooling system was evaluated in terms of required variation of the comfort condition of the users (internal temperature and, if possible, relative humidity) and payback loads in the electricity power curve. In particular, flexibility curves have been defined for each plant and they characterize the behavior of individual systems in terms of available flexibility: they quantify the pre-cooling period duration and the energy demand variation during a peak shaving event while varying the temperature comfort band and the peak shaving percentage. The flexibility curves help also to distinguish the different level of involvement of the two main flexibility sources, i.e., thermostatically controlled loads and thermal mass of the distribution system.

In this work the flexibility curves for the main technologies involved in the space cooling sector have been provided and the key conclusions derived from their analysis can be summarized as follows:

- The split system with on-off regulation shows a rather inflexible behavior during peak shaving events. Only peak annulments are possible with a high impact on the users indoor temperature setpoints before the event. In particular, to reduce to zero the electricity consumption in the peak time, a precooling of 2 °C for about 10 hours with an upper comfort band of 0.5 °C have to be adopted and this leads to 28.7 % increment of electricity consumption in the time before the event.
- Fan coil units coupled with a variable capacity heat pump are the most flexible system when the energy flexibility from thermostatically controlled loads (TCLs) is activated. To avoid great payback loads, it is advisable to allow the internal air temperature to rise during the event. For instance, allowing an increase of 1 °C in the air temperature, the electricity consumption can be reduced of 100 % in the peak time with a very low pre-cooling (from 0.5 to 2.25 hours in relation to the value of the minimum comfort band allowed to the setpoint) and no electricity increase in the time before the event. However, the addition of a thermal energy storage (e.g., a cold-water tank) to the distribution system allows to realize short term peak shaving strategies without compromising the indoor air temperature with low drawback effects in terms of anticipated electricity overconsumptions.
- As regards high massive cooling system, the storage capability of the distribution system allows the realization of different peak reduction events with a combined exploitation of the energy flexibility derived by thermostatically controlled loads (TCLs) and by its thermal mass. Results show that, as the thermal mass of the system increases (e.g., concrete ceiling cooling in comparison to ceiling panels), the flexibility of the thermostat is less and less exploited. However, increased anticipated overconsumption due to pre-cooling of the thermal mass of the system must be expected: above + 100 % for the concrete ceiling cooling regardless the comfort band, while for ceiling panels it assumes values near to + 35 % with a large comfort band or up to + 80 % for very narrow comfort band. Furthermore, the occurrence of power peaks delayed with respect to the event is also a drawback effect to be expected.
- When the level of thermal inertia of the emission system decreases, the activation of the energy flexibility from TCLs in the hours before the event allows to obtain also benefits in terms of electricity consumption reduction in the hours following the DR event. Such electricity saving is greater for FCU in the configuration without the TES (a reduction of 96 % can be reached) and decreases passing from CP (maximum energy saving of about 9 %) to CC, where no energy demand reduction occurs after the event.
- Comparing the flexibility sources exploited by the modelled space cooling systems, it is clear that the TCLs is the only resource available for the split and the FCU systems. The decrease in use of this resource occurs when the thermal inertia of the distribution system increases. Indeed, the exploitation of the TCLs decreases more and more passing by CP to CC at the expense of the thermal mass of the system. However, only in case of an FCU with TES is possible to avoid completely the TCLs exploitation when the electricity peak wants to be annulled. This is due to the decoupling of demand from generation which is only possible with a storage device added to the plant.

To conclude, the analysis shows that the type of emission system used to satisfy the cooling demand of a residential building has a considerable impact on how a programmed peak shaving event is handled. Therefore, taking this aspect into consideration, it is of paramount importance to improve the implementation of large-scale DSM strategies involving cooling systems. Indeed, the assessment of the electric power curve variations in the period before and after the event is crucial to plan a strategy by a hypothetical supervisor, diversified on the basis of users expected reactions.

At this aim, the introduced flexibility curves have proved to be an easy and fast instrument to summarize the space cooling dynamic in presence of a peak shaving Demand Response event.

NOMENCLATURE

Δk	Timestep (hours)
ΔT	Temperature difference (°C)
ΔRH	Relative humidity difference (%)
$\mathbf{A}$	State space model coefficient matrices for state vector
AC	Air cooling
$\mathbf{B}$	State space model coefficient matrices for input
BL	Baseload
C	Thermal capacity (kWh K^{-1})
$\mathbf{C}$	State space model coefficient matrices for state vector
CC	Concrete ceiling
CP	Ceiling panels
$CTRL$	Boolean control
$\mathbf{D}$	State space model coefficient matrices for input
DH	Dehumidifier
dk	Infinitesimal time difference
DR	Demand Response
DSM	Demand side management
EER	Energy efficiency ratio
f	Reduction factor
FCU	Fan coil unit
Flex	Flexibility curve (%)
$\dot{G}$	Gains (W)
h	Heat of evaporation (J kg_{vap}^{-1})
HP	Heat pump
K	Thermal conductance (W K^{-1})
k	Discrete time (hours)
L	Loss coefficient factor (W K^{-1})
MILP	Mixed -integer linear programming
M	Mass (kg)
$\dot{m}$	Flowrate (kg s^{-1})
$\dot{P}$	Electricity power (W_{el})
$\dot{P}^{*}$	Electricity power shift (%)
PSS	Peak shaving strategy
$\dot{Q}$	Thermal power (W_{th})
R	Thermal resistance (K W^{-1})
RH	Relative humidity
SC	Space cooling
SS	Split system
T	Temperature (°C)
t	Continuous time (s)
TES	Thermal energy storage
TMD	Thermal mass of the distribution system
$\boldsymbol{U}$	Input vector
$\boldsymbol{X}$	State vector

x	Absolute humidity ($kg_{vap}\ kg_{as}^{-1}$)
$\boldsymbol{Y}$	Output vector

SUBSCRIPTS

air	Internal air temperature
aDR	Time after the Demand Response event
bDR	Time before the Demand Response event
BL	Baseline
building	Thermal power to cover building demand
DH	Dehumidifier
DR	Demand Response
end	End time
env	Environment
f	Floor layer
fe	External floor layers
fi	Internal floor layers
fin	Thermal insulation floor layer
full-load	Full load operation
g	Ground
inf	Air infiltrations
int	Internal
l	Thermal losses
max	Maximum
min	Minimum
o	Outdoor
prec	Precooling time
PSS	Peak shaving strategy
rated	Rated conditions
r	Roof layers
re	External roof layers
RH	Relative humidity
ri	Internal roof layers
ri,ap	Internal roof layers (after ceiling panels, outwards)
ri,bp	Internal roof layers (before ceiling panels, inwards)
ri,cp	Internal roof layers (ceiling panels)
rin	Thermal insulation roof layer
s	Solar contribution
SC	Space cooling
shift	Shift power or energy
sp	Setpoint
start	Start time
T	Temperature
TES	Thermal energy storage
TMD	Thermal mass of the distribution system
v	Water vapor
w	Vertical walls layers
we	External vertical walls layers
wi	Internal vertical walls layers
win	Thermal insulation vertical walls floor layer

wind Windows

REFERENCES

[1] IEA, Cooling. More efforts needed., Track. Rep. (2020). iea.org/reports/cooling [accessed 7.04.2021].

[2] IEA, Energy Efficiency Indicators, Stat. Rep. (2020). iea.org/reports/energy-efficiency-indicators-overview [accessed 7.04.2021].

[3] L. Gelazanskas, K.A.A. Gamage, Demand side management in smart grid: A review and proposals for future direction, Sustain. Cities Soc. (2014). https://doi.org/10.1016/j.scs.2013.11.001.

[4] N. Oconnell, P. Pinson, H. Madsen, M. Omalley, Benefits and challenges of electrical demand response: A critical review, Renew. Sustain. Energy Rev. (2014). https://doi.org/10.1016/j.rser.2014.07.098.

[5] U.S.D. of E. (USDOE), Benefits of Demand Response in Electricity Markets and Recommendations for Achieving Them, (2006).

[6] A. Arteconi, N.J. Hewitt, F. Polonara, Domestic demand-side management (DSM): Role of heat pumps and thermal energy storage (TES) systems, Appl. Therm. Eng. (2013). https://doi.org/10.1016/j.applthermaleng.2012.09.023.

[7] W. Li, L. Yang, Y. Ji, P. Xu, Estimating demand response potential under coupled thermal inertia of building and air-conditioning system, Energy Build. (2019). https://doi.org/10.1016/j.enbuild.2018.10.022.

[8] C. Yan, F. Wang, Y. Pan, K. Shan, R. Kosonen, A multi-timescale cold storage system within energy flexible buildings for power balance management of smart grids, Renew. Energy. (2020). https://doi.org/10.1016/j.renene.2020.07.079.

[9] A. Arteconi, J. Xu, E. Ciarrocchi, L. Paciello, G. Comodi, F. Polonara, R. Wang, Demand Side Management of a Building Summer Cooling Load by Means of a Thermal Energy Storage, in: Energy Procedia, 2015. https://doi.org/10.1016/j.egypro.2015.07.705.

[10] R. Tang, S. Wang, C. Yan, A direct load control strategy of centralized air-conditioning systems for building fast demand response to urgent requests of smart grids, Autom. Constr. (2018). https://doi.org/10.1016/j.autcon.2017.12.012.

[11] A. Malik, N. Haghdadi, I. MacGill, J. Ravishankar, Appliance level data analysis of summer demand reduction potential from residential air conditioner control, Appl. Energy. (2019). https://doi.org/10.1016/j.apenergy.2018.11.010.

[12] N. Qi, L. Cheng, H. Xu, K. Wu, X.L. Li, Y. Wang, R. Liu, Smart meter data-driven evaluation of operational demand response potential of residential air conditioning loads, Appl. Energy. (2020). https://doi.org/10.1016/j.apenergy.2020.115708.

[13] S. Huang, D. Wu, Validation on aggregate flexibility from residential air conditioning systems for building-to-grid integration, Energy Build. (2019). https://doi.org/10.1016/j.enbuild.2019.07.043.

[14] A. Arteconi, A. Mugnini, F. Polonara, Energy flexible buildings: A methodology for rating the flexibility performance of buildings with electric heating and cooling systems, Appl. Energy. (2019). https://doi.org/10.1016/j.apenergy.2019.113387.

[15] A. Mugnini, F. Polonara, A. Arteconi, Quantification of energy flexibility from air conditioning of residential buildings, in: Refrig. Sci. Technol., 2019. 10.18462/iir.icr.2019.966.

[16] S.J. Pedersen CO, Fisher DE, ASHRAE. Cooling and heating load calculation principles., 1998.

[17] A. Boodi, K. Beddiar, Y. Amirat, M. Benbouzid. Simplified Building Thermal Model Development and Parameters Evaluation Using a Stochastic Approach, Energies. 13(11), 2899 (2020). doi.org/10.3390/en13112899

[18] Un.E. ISO, EN ISO 13790. Energy performance of buildings Calculation of energy use for space heating and cooling, (2008) 1–24.

[19] W.D. Dieter Patteeuw, Kenneth Bruninx, Alessia Arteconi, Erik Delarue, L. Helsen, Integrated modeling of active demand response with electric heating systems coupled to thermal energy storage systems, Appl. Energy. 151 (2015) 306–319. doi.org/10.1016/j.apenergy.2015.04.014.

[20] TRNSYS, TRNSYS 17 Documentation, Univ. Wisconsin-Madison. (2012).

[21] W. Cui, Y. Ding, H. Hui, M. Li, Two-stage payback model for the assessment of curtailment services provided by air conditioners, in: Energy Procedia, 2017. doi.org/10.1016/j.egypro.2017.12.409.

[22] V. Corrado, I. Ballarini, S.P. Corgnati, Typology Approach for Building Stock: D6.2 National scientific report on the TABULA activities in Italy, 2012.

[23] UNI/TR 11552, Opaque envelope components of buildings Thermo-physical parameters, (2014) 1–44.

[24] Weather Data. energyplus.net/weather [accessed 7.04.2021].

[25] Viessmann, VITOCELL 100-E/-W, Commer. Cat. www.viessmann.it/it/riscaldamento-casa/bollitori-e-serbatoi-per-acqua-calda/serbatoi-accumulo-acqua-di-riscaldamento/vitocell-100ew.html [accessed 7.04.2021].

[26] Viessmann, VITOCAL 200-S, Commer. Cat. www.viessmann.it/it/riscaldamento-casa/pompe-di-calore/pompe-di-calore-aria-acqua-split/vitocal-200-s.html [accessed 7.04.2021].

[27] R. Group, ECOdry CN+. Dehumidifier for radiant cooling., www.rossatogroup.com/prodotti/trattamento-aria/deumidificatori-radiante/deumidificatore-radiante-controsoffitto.html [accessed 7.04.2021].

APPENDIX A:

Fan coil units (FCUs) with variable capacity heat pump (no TES configuration)

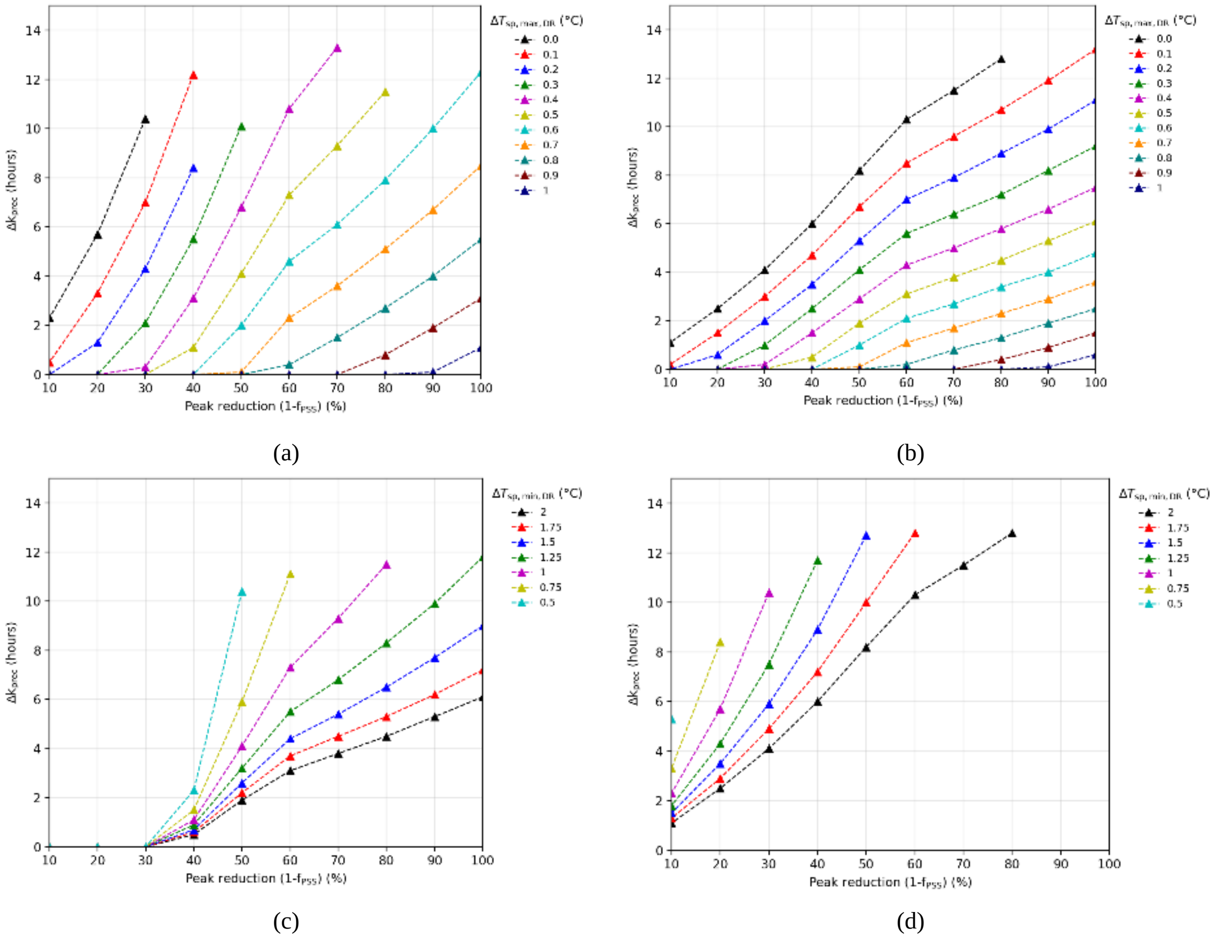

(a) (b)

(c) (d)

Figure A1. Flexibility curve: pre-cooling of the internal air node duration (Δk_{prec}) for FCU without TES for different peak reductions (f_{PSS}): (a) $\Delta T_{sp,min,DR}$ equal to 1 °C and variable $\Delta T_{sp,max,DR}$, (b) $\Delta T_{sp,min,DR}$ equal to 2 °C and variable $\Delta T_{sp,max,DR}$, (c) $\Delta T_{sp,max,DR}$ equal to 0.5 °C and variable $\Delta T_{sp,min,DR}$ and (d) $\Delta T_{sp,max,DR}$ equal to 0 °C and variable $\Delta T_{sp,min,DR}$.

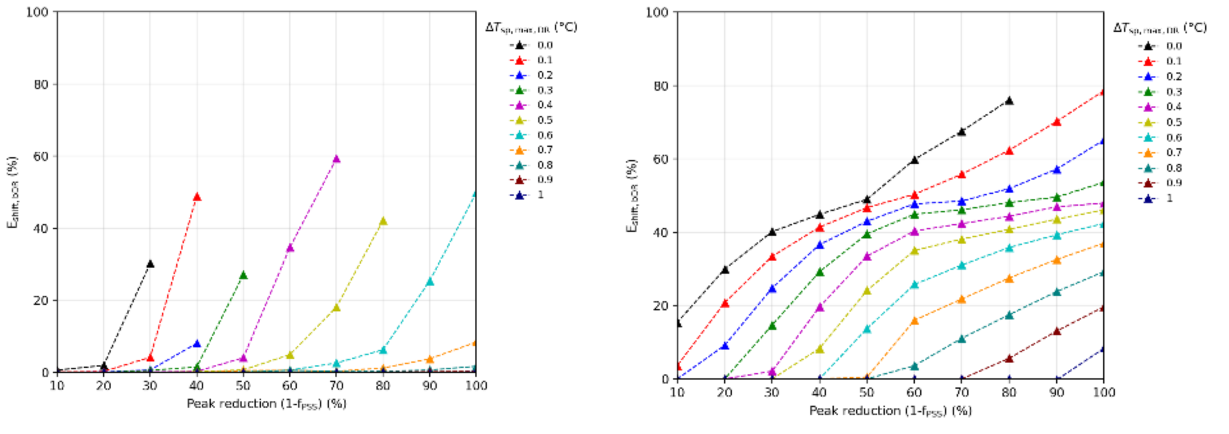

(a) (b)

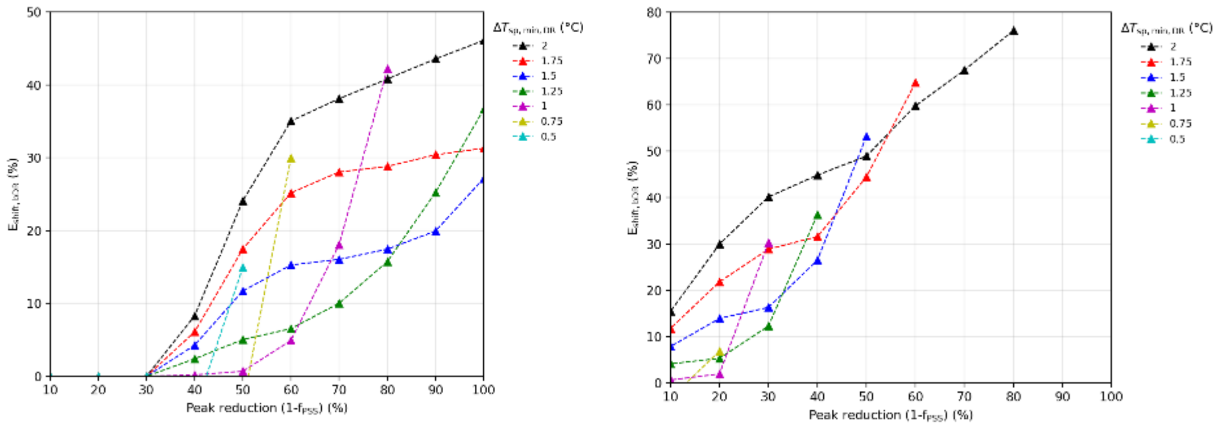

(c) (d)

Figure A2. Flexibility curve: $E_{shift,bDR}$ for FCU without TES for different peak reductions (f_{PSS}): (a) $\Delta T_{sp,min,DR}$ equal to 1 °C and variable $\Delta T_{sp,max,DR}$, (b) $\Delta T_{sp,min,DR}$ equal to 2 °C and variable $\Delta T_{sp,max,DR}$, (c) $\Delta T_{sp,max,DR}$ equal to 0.5 °C and variable $\Delta T_{sp,min,DR}$ and (d) $\Delta T_{sp,max,DR}$ equal to 0 °C and variable $\Delta T_{sp,min,DR}$.

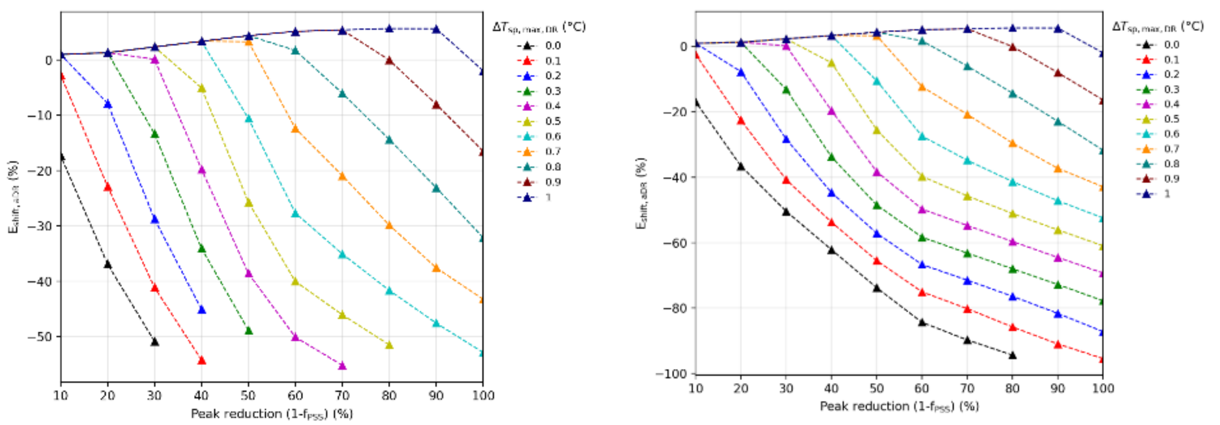

(a) (b)

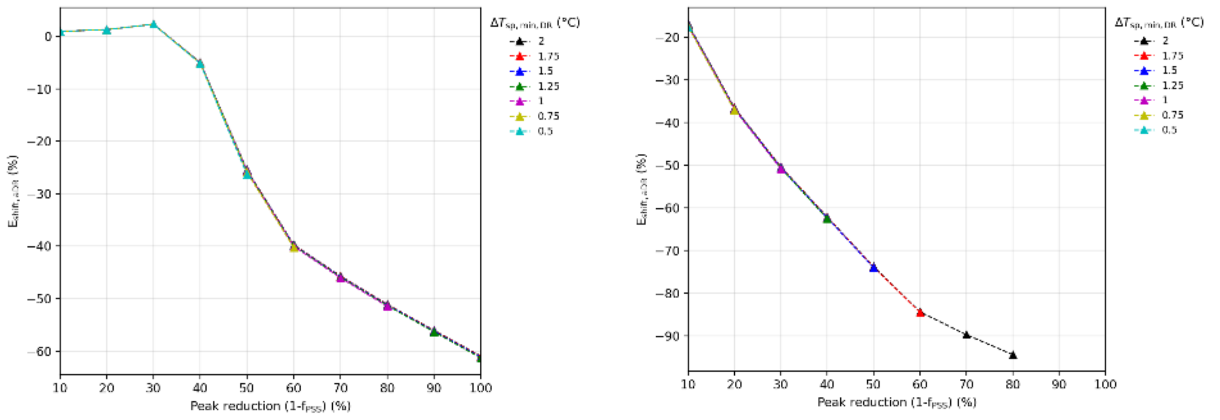

(c) (d)

Figure A3. Flexibility curve: $E_{shift,aDR}$ for FCU without TES for different peak reductions (f_{PSS}): (a) $\Delta T_{sp,min,DR}$ equal to 1 °C and variable $\Delta T_{sp,max,DR}$, (b) $\Delta T_{sp,min,DR}$ equal to 2 °C and variable $\Delta T_{sp,max,DR}$, (c) $\Delta T_{sp,max,DR}$ equal to 0.5 °C and variable $\Delta T_{sp,min,DR}$ and (d) $\Delta T_{sp,max,DR}$ equal to 0 °C and variable $\Delta T_{sp,min,DR}$.

APPENDIX B:

Cooling ceiling panels (CP) with dehumidifier (DH)

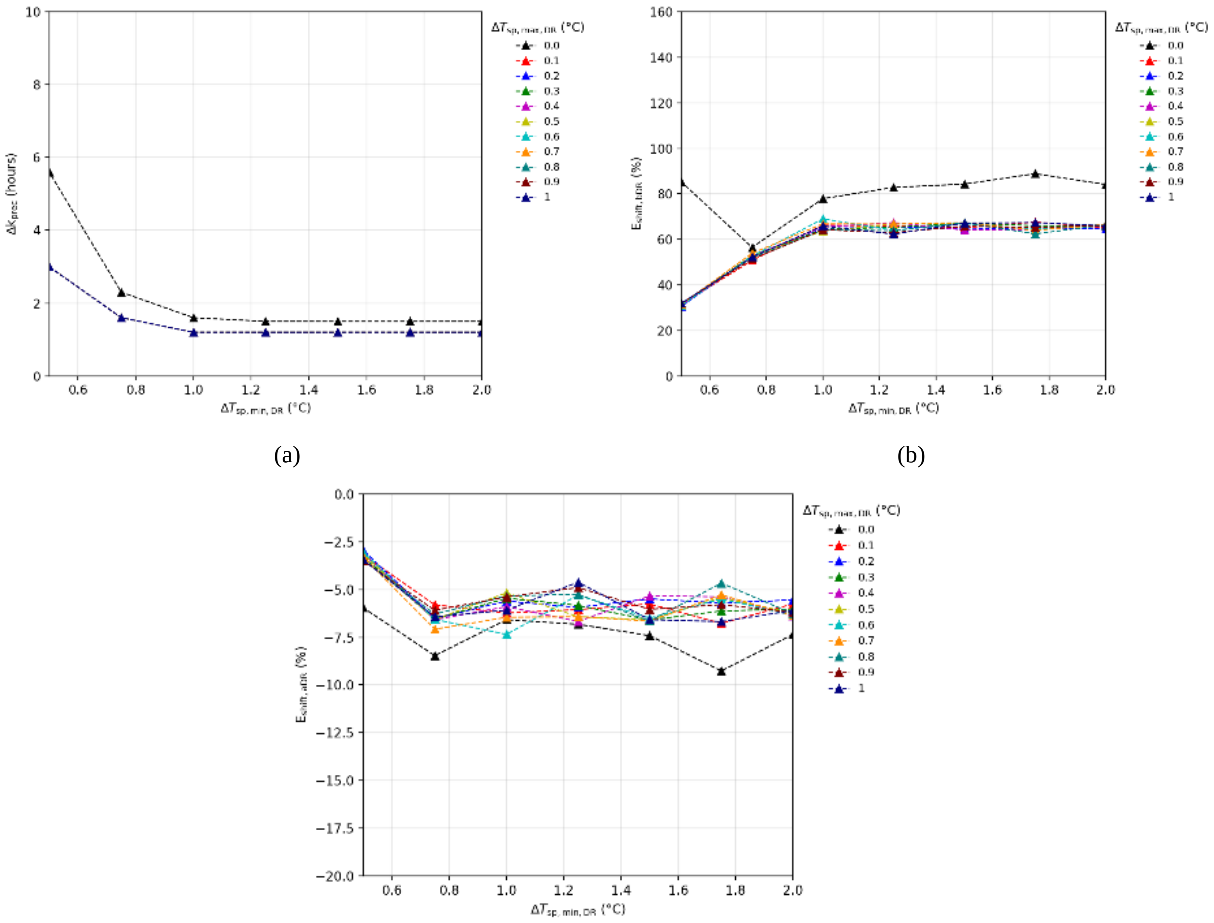

(a) (b)

(c)

Figure B1. Daily flexibility curves for an event with f_{PSS} equal to 0 (100% peak reduction) and Δk_{DR} of 1 hour as the $\Delta T_{sp,max,DR}$ and $\Delta T_{sp,min,DR}$ vary for CP ($\Delta RH_{sp,max,DR}$ and $\Delta RH_{sp,min,DR}$ equal to 10 %): (a) Pre-cooling of the internal air node duration (Δk_{prec}), (b) $E_{shift,bDR}$ and (c) $E_{shift,aDR}$

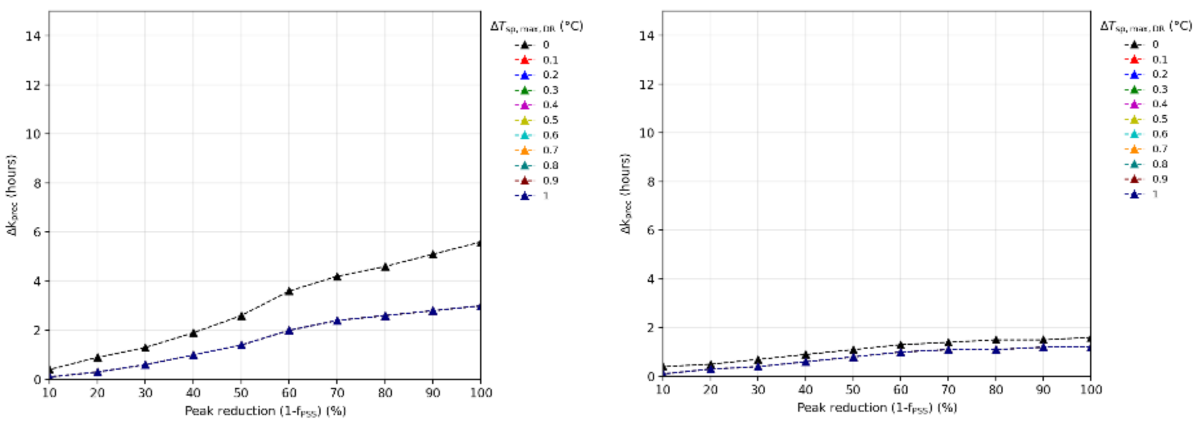

(a) (b)

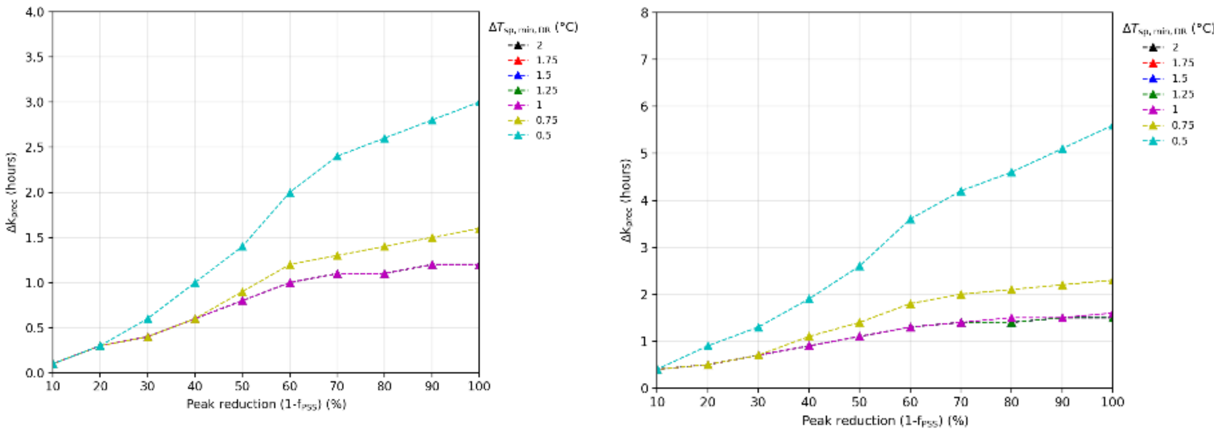

(c) (d)

Figure B2. Flexibility curve: Pre-cooling of the internal air node duration (Δk_{prec}) for CP for different peak reductions (f_{PSS}): (a) $\Delta T_{sp,min,DR}$ equal to 0.5 °C and variable $\Delta T_{sp,max,DR}$, (b) $\Delta T_{sp,min,DR}$ equal to 1 °C and variable $\Delta T_{sp,max,DR}$, (c) $\Delta T_{sp,max,DR}$ equal to 0.5 °C and variable $\Delta T_{sp,min,DR}$ and (d) $\Delta T_{sp,max,DR}$ equal to 0 °C and variable $\Delta T_{sp,min,DR}$. All the figures are realized with $\Delta RH_{sp,max,DR}$ equal to 5 %.

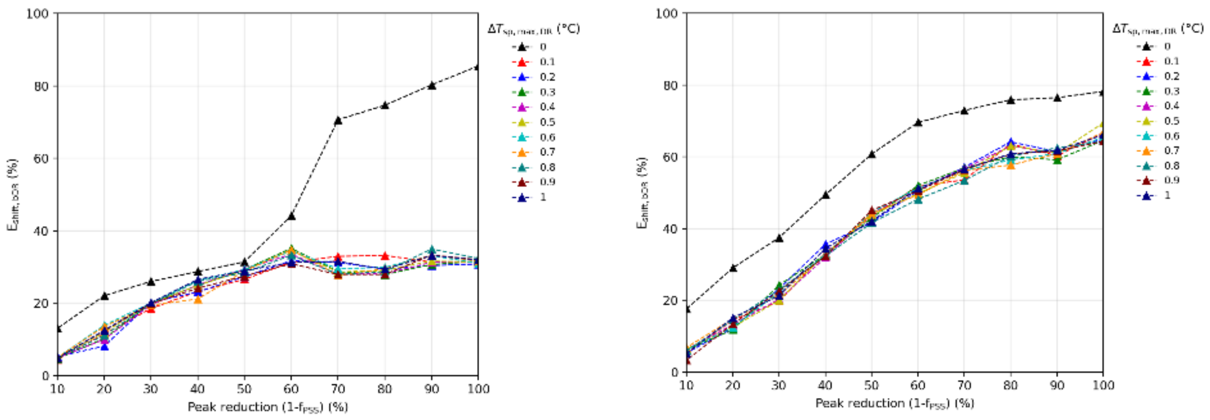

(a) (b)

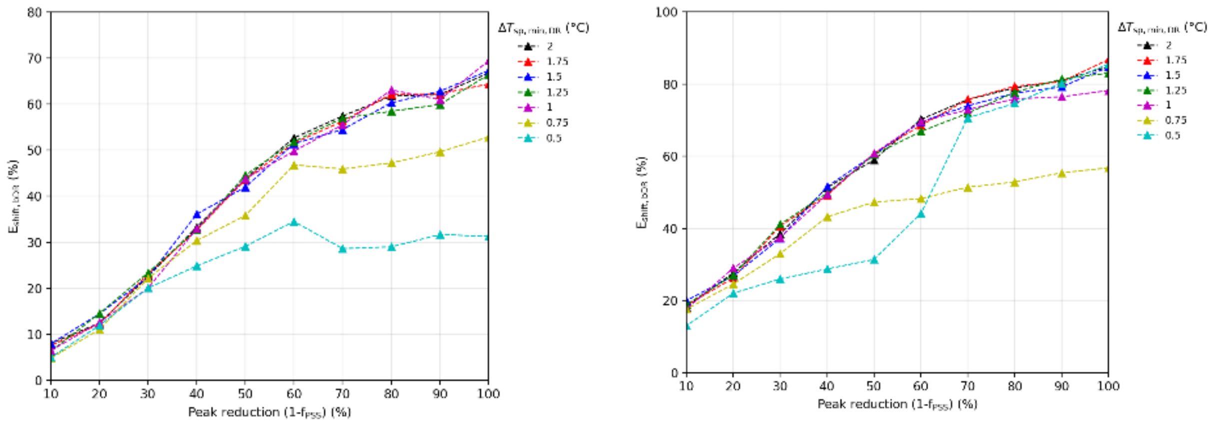

(c) (d)

Figure B3. Flexibility curve: $E_{shift,bDR}$ for CP for different peak reductions (f_{PSS}): (a) $\Delta T_{sp,min,DR}$ equal to 0.5 °C and variable $\Delta T_{sp,max,DR}$, (b) $\Delta T_{sp,min,DR}$ equal to 1 °C and variable $\Delta T_{sp,max,DR}$, (c) $\Delta T_{sp,max,DR}$ equal to 0.5 °C and variable $\Delta T_{sp,min,DR}$ and (d) $\Delta T_{sp,max,DR}$ equal to 0 °C and variable $\Delta T_{sp,min,DR}$. All the figures are realized with $\Delta RH_{sp,max,DR}$ equal to 5 %.

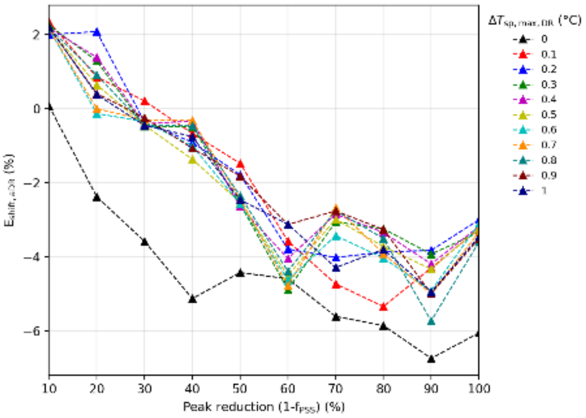

(a)

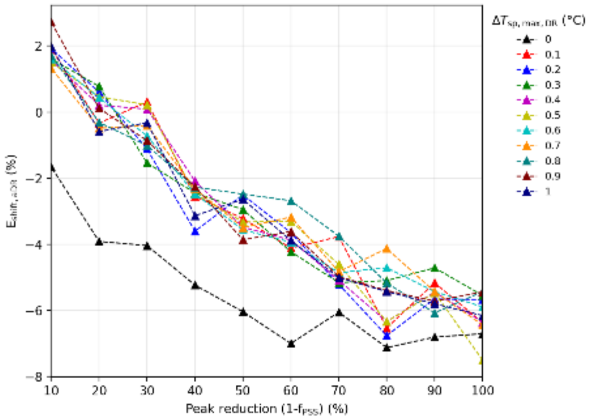

(b)

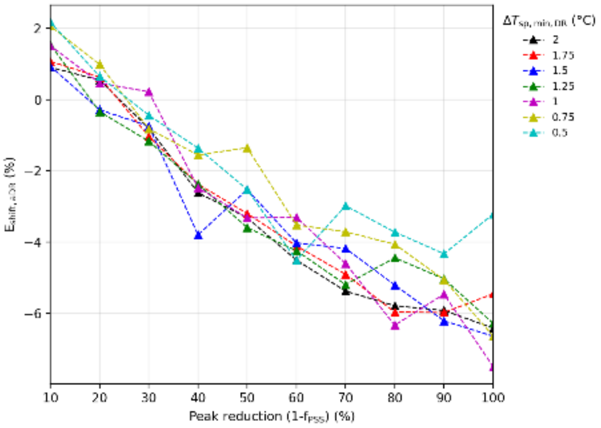

(c)

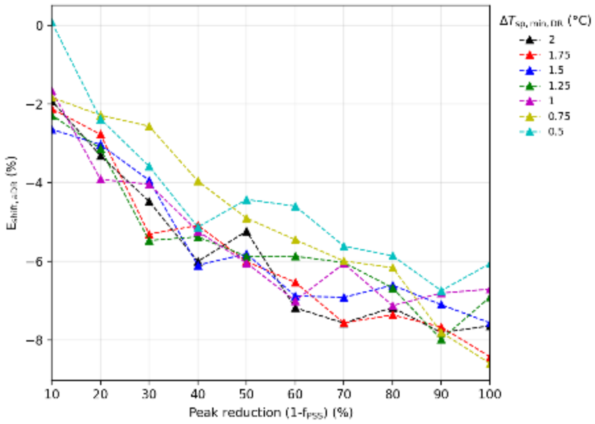

(d)

Figure B4. Flexibility curve: $E_{shift,aDR}$ for CP for different peak reductions (f_{PSS}): (a) $\Delta T_{sp,min,DR}$ equal to 0.5 °C and variable $\Delta T_{sp,max,DR}$, (b) $\Delta T_{sp,min,DR}$ equal to 1 °C and variable $\Delta T_{sp,max,DR}$, (c) $\Delta T_{sp,max,DR}$ equal to 0.5 °C and variable $\Delta T_{sp,min,DR}$ and (d) $\Delta T_{sp,max,DR}$ equal to 0 °C and variable $\Delta T_{sp,min,DR}$. All the figures are realized with $\Delta RH_{sp,max,DR}$ equal to 5 %.

APPENDIX C

Cooling concrete ceiling (CC) with dehumidifier (DH)

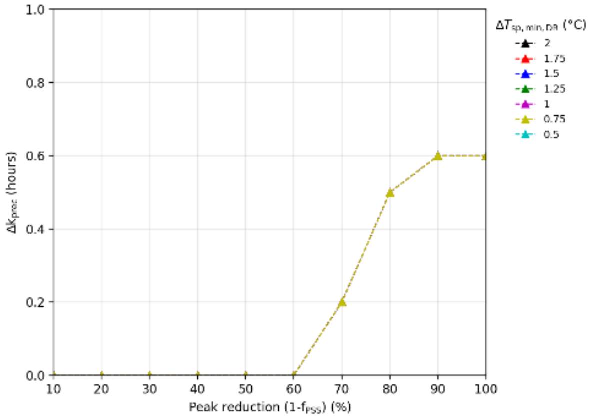

(a)

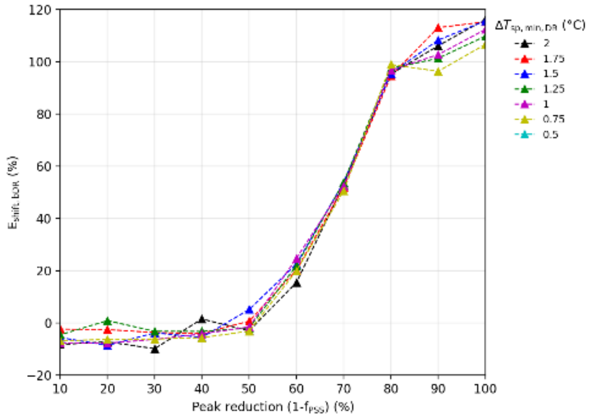

(b)

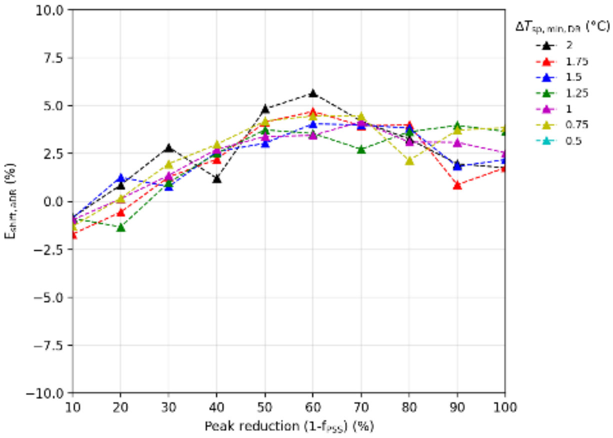

(c)

Figure C1. Daily flexibility curves for an event with $\Delta T_{sp,max,DR}$ equal to 1 °C and Δk_{DR} of 1 hour as the $\Delta T_{sp,min,DR}$ and the peak reduction (f_{PSS}) vary for CC ($\Delta RH_{sp,max,DR}$ and $\Delta RH_{sp,min,DR}$ equal to 5 %): (a) Pre-cooling of the internal air node duration (Δk_{prec}), (b) $E_{shift,bDR}$ and (c) $E_{shift,aDR}$.

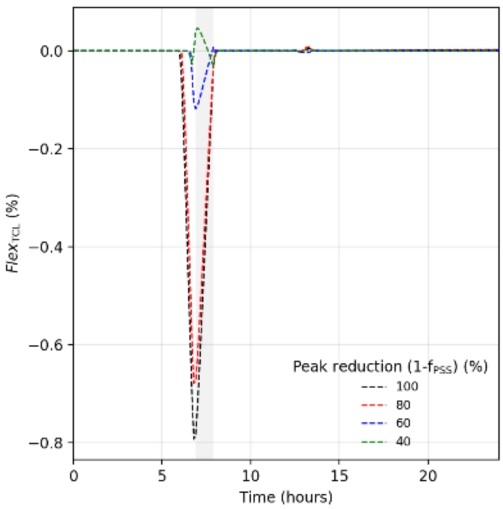

(a)

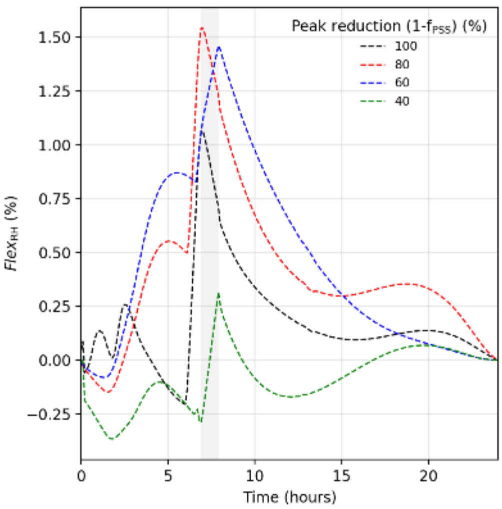

(b)

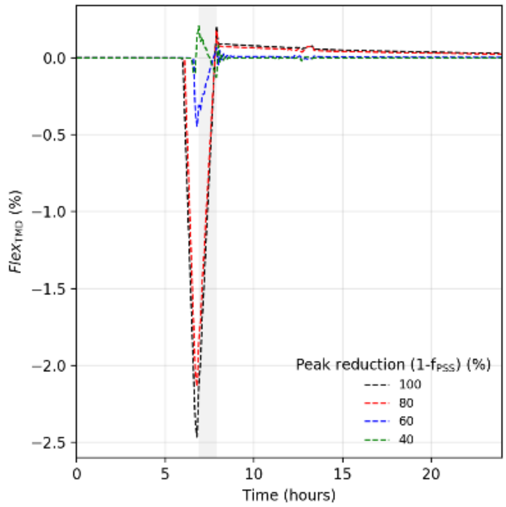

(c)

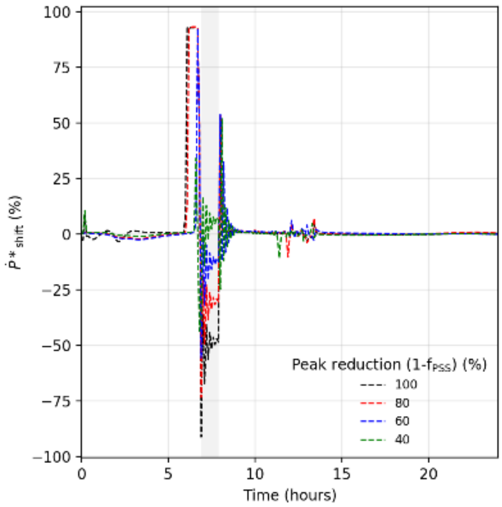

(d)

Figure C2. Daily demand response operation (f_{PSS} of 0, 0.2, 0.4 and 0.6, Δk_{DR} of 1 hour, $\Delta T_{sp,max,DR}$ of 1 °C and $\Delta T_{sp,min,DR}$ of 2 °C) for CC ($\Delta RH_{sp,max,DR}$ and $\Delta RH_{sp,min,DR}$ equal to 5 %): (a) $Flex_{TCL}$, (b) $Flex_{RH}$, (c) $Flex_{TMD}$ and (c) $\dot{P}^*_{shift}$.

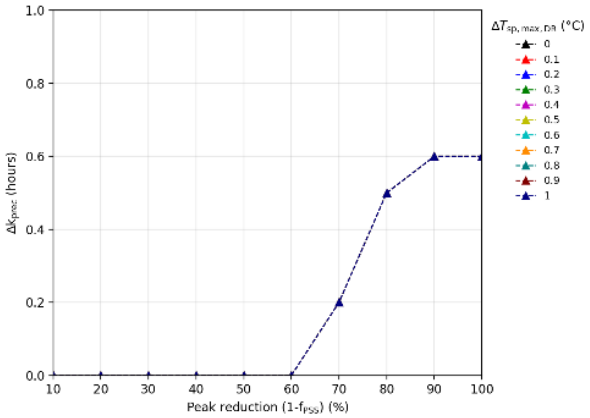

(a)

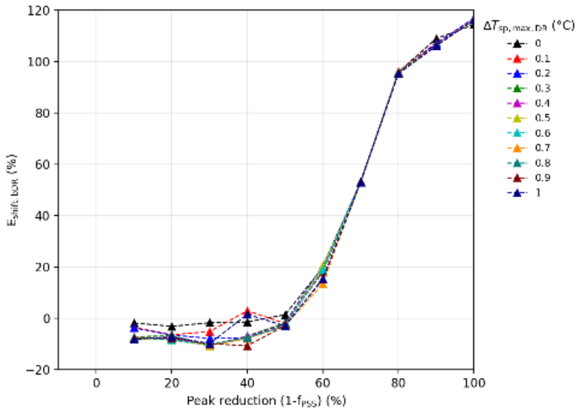

(b)

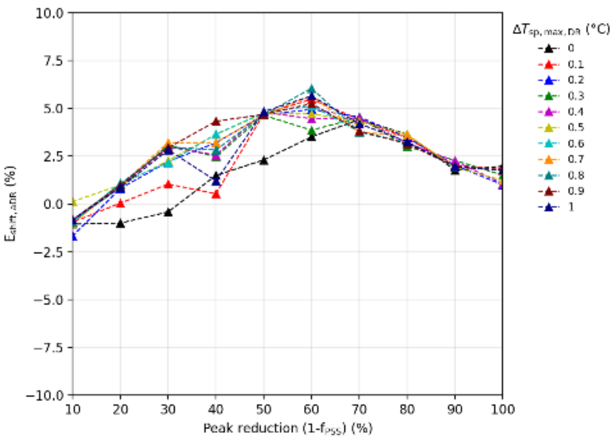

(c)

Figure C3. Daily flexibility curves for an event with $\Delta T_{sp,min,DR}$ equal to 2 °C and Δk_{DR} of 1 hour as the $\Delta T_{sp,axn,DR}$ and the peak reduction (f_{PSS}) vary for CC ($\Delta RH_{sp,max,DR}$ and $\Delta RH_{sp,min,DR}$ equal to 5 %): (a) Pre-cooling of the internal air node duration (Δk_{prec}), (b) $E_{shift,bDR}$ and (c) $E_{shift,aDR}$.